DOCTORAL THESIS

Reliability-based assessment of concrete dams considering combined sliding and overturning

Adrian Ulfberg

Structural Engineering

LULEÅ UNIVERSITY OF TECHNOLOGY

DOCTORAL THESIS

Reliability-based assessment of concrete dams considering combined sliding and overturning

Adrian Ulfberg

Luleå 2025

Luleå University of Technology
Department of Civil, Environmental and Natural Resources Engineering
Division of Structural and Fire Engineering
SE-971 87 Luleå, Sweden
www.ltu.se

Printed by Luleå University of Technology, 2025.
ISSN: 1402-1544
ISBN: 978-91-8048-953-9 (print)
ISBN: 978-91-8048-954-6 (electronic)

Luleå 2025
www.ltu.se

Adrian Ulfberg
Division of Structural and Fire Engineering
Department of Civil, Environmental and Natural Resources Engineering
Luleå University of Technology

Academic thesis

For the degree of Doctor of Philosophy (Ph.D.) in Structural Engineering, which by due permission of the Technical Faculty Board at Luleå University of Technology will be publicly defended in:

Room A117, Luleå University of Technology,

Tuesday, February 10th, 2026, 09:00

Opponent:	Professor Luis Altarejos-García, Universidad Politécnica de Cartagena
Examining Committee:	Professor Dan M. Frangopol, Lehigh University
	Professor Henrik Stang, Danmarks Tekniske Universitet
	Professor S.M. Samindi M.K. Samarakoon, Universitetet i Stavanger

Principal supervisor:	Professor Gabriel Sas, Luleå tekniska universitet
Assistant supervisors:	Associate Senior Lecturer Dr. Jaime González-Libreros, Luleå tekniska universitet
	Professor Fredrik Johansson, Kungliga Tekniska högskolan
	Doctor Marie Westberg Wilde, Kungliga Tekniska högskolan & AFRY
	Docent Richard Malm, Totalförsvarets forskningsinstitut
	Associate Senior Lecturer Dr. Chao Wang, Luleå tekniska universitet

Preface

Firstly, I would like to gratefully acknowledge the Swedish Research Council for Sustainable Development and the Swedish Centre for Sustainable Hydropower for financing this project, which made the research presented in this thesis possible.

This thesis is the culmination of five years of research, a journey supported by my invaluable supervisors, whose guidance and input made this work possible. I would especially like to thank Prof. Gabriel Sas and Dr. Jaime González-Libreros for their encouragement, motivation, and committed support, as well as Prof. Fredrik Johansson and Dr. Marie Westberg Wilde for helping me navigate the field of dam engineering and for providing astute insights throughout this research.

I am grateful to all my other wonderful colleagues and friends at LTU, especially Silvia, for her encouragement and the many insightful discussions about reliability, Angélica, for her kindness and helpful attitude, and Flo, for all the cookies and fun games. I also thank Mats and Erik for their assistance and for making the lab a truly enjoyable and fun place. I am also grateful to everyone who helped and contributed to this work in any way, including the colleagues and acquaintances I have had the pleasure of getting to know at KTH, whose interactions and contributions have enriched this journey.

I sincerely thank my parents, my sisters, my brother, and my grandmother for their encouragement and care, both of which have been invaluable to me. To Sarah, thank you for your support during the tough times, for your understanding through all the late nights and weekends of work, and for being there with me on this journey.

Adrian Ulfberg

Luleå, December 2025

Summary

This thesis aims to improve the assessment of dam safety through the formalization of an identified failure mode that combines the sliding and overturning failure mechanisms. The failure mode is relevant to dams with geometrical variations and large-scale asperities in the rock-concrete interface and represents the behavior observed in finite element analyses (FEA) and scale model tests.

Dams are vital infrastructure, providing services such as water storage for hydropower and irrigation, flood control, and containment of industrial byproducts. However, storing large volumes of water carries the risk of potentially catastrophic consequences in the event of failure, making safety assessments essential throughout a dam's service life. Regulatory rules and guidelines prescribe methods for performing such dam safety assessments, in which a dam's safety against global failure modes such as sliding and overturning is commonly evaluated. However, these failure modes rely on assumptions that may not be consistent with the actual behavior of dams when large-scale asperities are present along the rock-concrete interface, which may cause the dam to exhibit a failure mode that combines both sliding and overturning. Furthermore, these regulatory rules and guidelines typically employ deterministic assessment approaches, providing general safety factors that must be calibrated for specific cases to achieve the desired level of safety. Given that dams are unique structures with inherent uncertainties, this approach is unlikely to produce consistent safety levels.

The failure mode presented in this thesis, referred to as combined sliding and overturning (CSO), addresses the limitations of the traditional failure modes and reflects the failure behavior observed in concrete dams with large-scale asperities along the rock-concrete interface. Having been identified in FEA of concrete buttress dams, the failure mode was formalized and an analytical formulation was developed, providing results almost identical to those of FEA. The assumptions behind the failure mode and analytical formulation were compared with twelve scale model tests on concrete buttress dams, which included a monitoring system to validate these assumptions. The tests confirmed the assumptions and also evaluated the influence of factors such as rock bolts, reinforcement, and rock joints on load capacity and behavior, which primarily affected the load capacity.

By relying solely on equilibrium equations, like traditional failure modes, the analytical formulation provides a simple alternative to methods such as FEA and can be readily applied with reliability analysis to assess a dam's safety while accounting for its unique uncertainties. This is exemplified by a study on the reliability and sensitivity analysis of concrete buttress dams, in which a population of buttress dam monoliths, varying in height, width, and other characteristics, is generated and assessed for sliding, overturning, and CSO under two load cases, involving either overtopping or ice load. As such, influential factors for a dam's reliability, including the basic friction angle, the dilation angle, the monolith height, and the inclinations of the front plate and the large-scale asperities, were identified. By introducing original methods to assess a dam's load capacity while highlighting which factors impact the reliability of concrete dams, this thesis contributes to improved concrete dam safety assessment.

Keywords: Concrete dams, reliability analysis, sensitivity analysis, metamodeling, scale model testing, combined sliding and overturning.

Sammanfattning

Denna avhandling syftar till att förbättra bedömningen av dammsäkerhet genom formalisering av en brottmod som kombinerar glidning och stjälpning. Brottmoden är relevant för dammar med geometriska variationer och storskaliga bergklackar i kontaktytan mellan berg och betong och representerar det beteende som observerats i finita elementanalyser (FEA) och skalmodellförsök.

Dammar utgör kritisk infrastruktur och möjliggör vattenlagring för vattenkraft och bevattning, flödesreglering samt inneslutning av industriella restprodukter. Lagring av stora vattenvolymer medför dock en risk för potentiellt katastrofala konsekvenser vid ett dammhaveri, vilket gör säkerhetsbedömningar nödvändiga under hela dammens livslängd. Regelverk och riktlinjer föreskriver metoder för genomförande av sådana säkerhetsbedömningar, där dammens säkerhet mot globala brottmekanismer såsom glidning och stjälpning vanligtvis utvärderas. Dessa brottmoder bygger emellertid på antaganden som inte alltid är förenliga med dammars faktiska beteende när storskaliga bergklackar förekommer i kontaktytan mellan betong och berg, vilket kan leda till ett brottförlopp som kombinerar både glidning och stjälpning. Vidare tillämpar regelverk och riktlinjer i regel deterministiska analysmetoder, där generella säkerhetsfaktorer används och måste kalibreras för specifika fall för att uppnå önskad säkerhetsnivå. Eftersom dammar är unika konstruktioner med stora osäkerheter relaterade till material och last är detta tillvägagångssätt osannolikt att resultera i konsekventa säkerhetsnivåer.

Brottmoden som presenteras i denna avhandling kallas kombinerad glidning och stjälpning (combined sliding and overturning, CSO). Den adresserar begränsningarna hos de traditionella brottmoderna och återspeglar det brottbeteende som observerats i betongdammar med stora ojämnheter längs kontaktytan mellan berg och betong. Efter att ha identifierats i FEA av lamelldammar, formaliserades brottmoden och en analytisk formulering utvecklades, som ger resultat som överensstämmer med FEA. Antagandena för brottmoden och den analytiska formuleringen jämfördes med tolv skalmodellförsök på lamelldammar med ett mätsystem designat för att verifiera dessa antaganden. Försöken bekräftade antagandena och utvärderade även inverkan av faktorer såsom bergsförankring, armering och bergsprickor på lastkapacitet och beteende, vilka huvudsakligen påverkade lastkapaciteten.

Genom att, likt traditionella brottmoder, enbart baseras på jämviktsekvationer är den analytiska formuleringen ett enkelt alternativ till metoder såsom FEA och kan enkelt kombineras med tillförlitlighetsanalys för att bedöma en dams säkerhet. Detta illustreras genom en tillförlitlighets- och känslighetsanalys för lamelldammar, där en population av lamelldammsmonoliter med varierande höjd, bredd och andra egenskaper genereras och

analyseras för glidning, stjälpning och CSO för två lastfall, som innefattar antingen islast eller en vattennivå över dammkrönet. Där identifierades basfriktionen, dilatationsvinkel, lutningen för frontplattan och bergklackarna samt monolitens höjd som viktiga faktorer för en lamelldamms säkerhet. Genom att introducera nya metoder för att bedöma en dams lastkapacitet och samtidigt belysa vilka faktorer som påverkar tillförlitligheten hos betongdammar, bidrar denna avhandling till förbättrade metoder för säkerhetsbedömning av betongdammar.

Table of Contents

List of Abbreviations

Abbreviation	Description
CDF	Cumulative Distribution Function
CSO	Combined Sliding and Overturning
DIC	Digital Image Correlation
FEA	Finite Element Analysis
FORM	First-Order Reliability Method
FOS	Fiber Optic Sensor
LHS	Latin Hypercube Sampling
LSF	Limit State Function
LVDT	Linear Variable Differential Transformer
MCS	Monte Carlo Simulation
MPP/MPFP	Most Probably Failure Point
NLFEA	Nonlinear Finite Element Analysis
PCE	Polynomial Chaos Expansion
PC-Kriging	Polynomial-Chaos-Kriging
PDF	Probability Density Function
QMC	Quasi-Monte Carlo
RSM	Response Surface Method
SORM	Second-Order Reliability Method
SVM	Support Vector Machines

Chapter 1

1. Introduction

This chapter outlines the purpose, scope, aim, objectives, hypothesis, research questions, and appended papers that form the foundation of this thesis. It also discusses the limitations and scope of the research, as well as the thesis outline and additional publications to which the author has contributed.

1.1 Purpose, Scope, and Aim

Purpose

The purpose of this thesis is to contribute to improved assessment of concrete dams by proposing alternative methods to those in current practices, whose shortcomings may lead to inaccurate or overly conservative safety estimates. Traditional sliding and overturning failure modes are evaluated deterministically and do not explicitly account for geometrical irregularities or large-scale asperities at the rock-concrete interface, which have been found to influence the failure behavior of concrete dams and significantly increase their load capacity. To address these issues, this thesis introduces an original failure mode, referred to as combined sliding and overturning (CSO), with a corresponding analytical formulation that can be readily used in reliability analysis, along with the parameters that significantly influence reliability when employing the CSO formulation.

Scope

While it is acknowledged that dams can fail in multiple ways, the research presented in this thesis primarily focuses on the global stability of individual dam monoliths or sections to address limitations identified in current global stability analysis practices. Although several types of dams exist and various loads can arise from different phenomena, particular attention is given here to concrete buttress dams subjected to static loads such as hydrostatic pressure, ice load, uplift, self-weight, and reaction forces from rock bolts. However, the results and the CSO failure mode, along with its analytical formulation presented in this thesis, may not be limited solely to buttress dams or static loads, as the main assumptions regarding failure behavior may be generally valid for concrete dams on uneven rock-concrete interfaces. Although dam safety is a broad and nuanced field, encompassing extensive programs involving activities such as monitoring and maintenance, this thesis focuses on the structural analysis aspect. In this thesis, the focus is also on the probability of failure, or its complement, reliability, while recognizing that safety should reflect both the probability of an event occurring and its consequences.

Aim

The aim of this thesis is to improve the accuracy of safety assessments of concrete dams.

1.2 Hypothesis and Objectives

Objectives

The objectives of this thesis were:

i. Identify the shortcomings of current assessment practices that may lead to conservative estimates when applied to concrete dams with large-scale asperities.
ii. Assess the influence of large-scale asperities on the behavior and load capacity of concrete dams.
iii. Investigate how the beneficial effect of large-scale asperities can be included in assessment.
iv. Conduct reliability and sensitivity analyses to determine the influential parameters for the safety of concrete dams with large-scale asperities in the rock-concrete interface.

Hypothesis

A concrete buttress dam's load capacity and safety can be more accurately estimated using reliability analysis in combination with finite element analysis (FEA) or the analytical formulation for CSO, both of which account for the influence of geometrical irregularities and large-scale asperities at interfaces.

1.3 Research Questions

The research questions addressed in this thesis are:

(i) How do geometrical irregularities and large-scale asperities in the rock-concrete interface affect a concrete buttress dam's potential failure behavior?
(ii) How can geometrical irregularities and large-scale asperities in the rock-concrete interface be accounted for in load capacity assessment of concrete buttress dams?
(iii) Which parameters related to the resistance and geometry of a buttress dam are most influential for its reliability?

1.4 Scientific Approach

To fulfill the objectives and address the research questions related to the thesis, a structured and incremental scientific approach was adopted that began with a literature review. This literature review focused on dam assessment practices, scale model testing, reliability analysis, and sensitivity analysis and was conducted to establish a foundation of knowledge and an understanding of the state of the art in these areas. The extensive literature review is presented in summarized form in Chapter 2.

Building on the literature review, the studies presented in Chapter 3 were devised to investigate the influence of geometrical irregularities and large-scale asperities in the rock-concrete interface of dams and to explore how these effects can be incorporated into assessments. To first gain an understanding of the influence of large-scale asperities on the failure behavior and load capacity of concrete dams, the studies presented in Papers I-II were developed, in which FEA simulations were used to determine the load capacity of dams with large-scale asperities at the rock-concrete interface.

Recognizing a distinct and consistent behavior in the FEA simulations with large-scale asperities in the rock-concrete interface in Papers I-II, characterized by simultaneous horizontal translation, rotation, and stress concentrations, a failure mode combining sliding and overturning was formalized and modeled analytically. The failure mode and its corresponding analytical formulation form the core of the study presented in Paper III, where they are compared with results from linear-elastic FEA and previously reported results from scale model tests.

To validate the assumptions of the developed failure mode beyond idealized, linear-elastic FEA, scale model tests were designed with a monitoring system to study the models' failure behavior and the evolution of strains. Furthermore, these scale model tests, presented in Paper IV, incorporated features such as rock bolts, reinforcement, and rock joints, which allowed their influence on failure behavior to be assessed and compared against the developed failure mode.

To better understand how different parameters affect the formalized failure mode, a reliability and sensitivity analysis was conducted. The study, presented in Paper V, calculates reliability and sensitivity measures for every sample in a simulated buttress dam monolith population, varying in design, for both the developed failure mode and the traditional failure modes from current practice. This approach of evaluating a population overcomes the potential issue of identifying parameters that are only important for a specific monolith design and allows the identification of parameters that are generally important.

The scientific approach to work presented in this thesis is summarized in Figure 1.

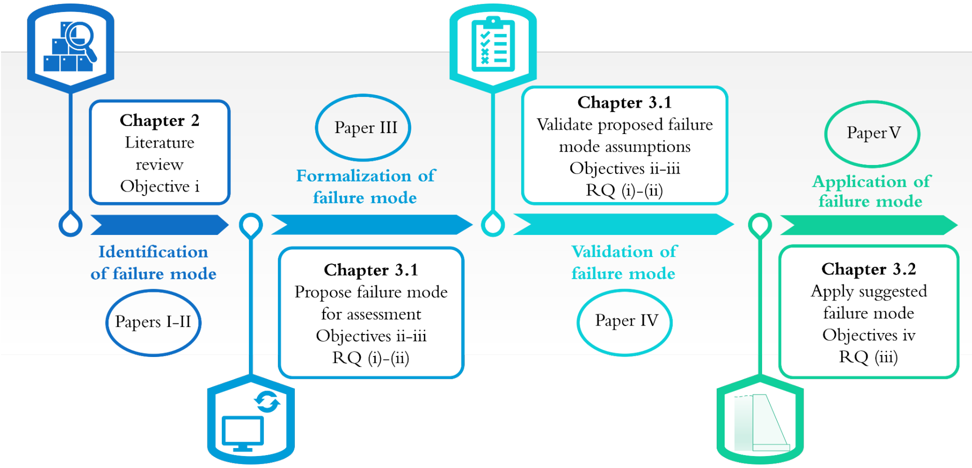

Figure 1 Scientific approach.

1.5 Limitations

The work contained in this thesis is subjected to several limitations that should be addressed:

- The thesis focuses only on studies involving concrete buttress dams with free-standing monoliths.
- Three-dimensional effects, including interactions between neighboring monoliths, were disregarded, and analyses were limited to static loads only.
- The foundation is assumed to be hard, crystalline rock with high bearing capacity and devoid of aspects such as rock joints that may affect the load capacity, unless explicitly mentioned.
- Cohesion and tensile strength of interfaces were disregarded throughout all research studies due to their inherent uncertainty and difficulties with reproducibility.
- While acknowledging epistemic uncertainty, which can be reduced through additional data or more refined models, such as by decreasing the degree of idealization, the uncertainties in this work are mainly treated as aleatoric, that is, as inherent randomness.
- The employed distribution functions and their corresponding means and standard deviations for random variables are obtained based on limited information, introducing epistemic uncertainties.

- While the scale model tests were carefully designed, created, and conducted, complete adherence to the scaling laws is virtually impossible, which may have slightly affected the results.

1.6 Outline of the Thesis

This is a compilation thesis, composed of an extended summary followed by appended research papers. This summary consists of five chapters, briefly described as follows:

Chapter 1 – Introduction outlines the aim and purpose of the research, along with the objectives and research questions, and describes the scientific approach adopted to address these. It also discusses the scope and limitations of the research and introduces the appended papers.

Chapter 2 – Literature review summarizes studies relevant to the core of the thesis, including analytical dam assessment practices, scale model testing, FEA, reliability analysis, and sensitivity analysis. It also provides background for the work presented in this thesis, placing the research in a broader context.

Chapter 3 – Load capacity and reliability assessment with combined sliding and overturning summarizes and discusses the results of the appended papers, and presents the CSO failure mode, its analytical formulation, and its application in dam safety assessment via reliability analysis. The failure mode was formalized during the research for this thesis and aims to amend the shortcoming of not considering large-scale asperities as in the current practices discussed in Chapter 2.

Chapter 4 – Conclusions summarize the main contributions of the research, provides answers to the research questions, and discusses the hypothesis.

Chapter 5 – Future research highlights the key research gaps identified in this work, which, if addressed, could enhance the safety assessment of concrete dams.

1.7 Appended Papers

The core of this thesis consists of five papers, three published journal articles and two submitted to journals, all introduced here together with the author's contribution.

PAPER I

Ulfberg, A., Gonzalez-Libreros, J., Das, O., Bista, D., Westberg Wilde, M., Johansson, F., Sas, G. (2023). Probabilistic finite element analysis of failures in concrete dams with large asperities in the rock-concrete interface. *Archives of Civil and Mechanical engineering*, 23, 109. Doi.org/10.1007/s43452-023-00652-4

The paper presents a probabilistic nonlinear finite element analysis (NLFEA) study on the influence of material parameters on the load capacity of scale model tests on dams with large-scale asperities in the interface that failed by cracking. By varying the modulus of elasticity, tensile strength, compressive strength, and fracture energy, the most influential parameters for the failure and load capacity were investigated. The author of this thesis contributed to the paper by writing the original draft, modelling and post-processing the NLFEA, and reviewing and editing the published work.

PAPER II

Bista, D., **Ulfberg, A**., Lia, L., Gonzalez-Libreros, J., Johansson, F., Sas, G. (2024). Numerical parametric study on the influence of location and inclination of large-scale asperities on the shear strength of concrete-rock interfaces of small buttress dams. *Journal of Rock Mechanics and Geotechnical Engineering*, Doi.org/10.1016/j.jrmge.2023.12.036

The paper presents a numerical parametric study on the influence of the location and inclination of a large-scale asperity in the rock-concrete interface on the load capacity of a concrete buttress dam. Using NLFEA, the study evaluates the failure behavior of buttress dams and simulates the various failures that may occur for different positions and inclinations, including global stability, buttress cracking, and failure of the large-scale asperity. The author of this thesis contributed to the paper by co-writing the original draft, modelling and post-processing the NLFEA simulations, and reviewing and editing the published work.

PAPER III

Ulfberg, A., Gonzalez-Libreros, J., Westberg Wilde, M., Johansson, F., Sas, G. (2025). Analytical Assessment of Combined Sliding and Overturning Failure in Concrete Dams. *Structural Engineering International*, Doi.org/10.1080/10168664.2025.2555918

Building upon the observations related to failure behavior of the studies in Papers I-II, this paper formalizes the observed failure behavior by introducing a CSO failure mode, along with a corresponding analytical formulation to assess load capacity. The CSO failure mode accounts for geometrical irregularities and large-scale asperities in the interface and serves as an intermediate between the individual sliding and overturning failure modes. The analytical formulation is compared against FEA and results from previously reported scale model tests with one or more large-scale asperities. Furthermore, approaches to limit the load capacity with respect to excessive deformations are provided. This failure mode was formalized, the analytical formulation was developed, the study was planned and conducted, and the paper was written by the author of this thesis.

PAPER IV

Ulfberg, A., Gonzalez-Libreros, J., Westberg Wilde, M., Johansson, F., Sas, G. (2025). Behavior and Failure Mechanism of Scale Model Buttress Dams with Large-Scale Asperities in the Rock-Concrete Interface. [Submitted to journal]

Extending the findings in Paper III, this paper presents results from twelve physical 1:5 scale model tests of concrete buttress dams conducted to study their failure behavior. Using a monitoring system specifically designed to validate the assumptions of the failure mode introduced in Paper III, the failure behaviors of the scale models are compared with the assumed behavior of CSO. Furthermore, by implementing various configurations of rock bolts, reinforcement, and rock joints, their influence on failure behavior and load capacity is evaluated. The scale models were designed, constructed, and tested, and the paper was written by the author of this thesis.

PAPER V

Ulfberg, A., Gonzalez-Libreros, J., Westberg Wilde, M., Johansson, F., Sas, G. (2025). Sensitivity and Reliability Analysis of Concrete Buttress Dams. [Submitted to journal]

Recognizing the lack of reliability and sensitivity analyses of concrete buttress dams in the literature, this study conducts such analyses on a population of generated buttress dam monoliths. The design of the monoliths is based on Swedish buttress dam designs, and the monoliths in the population vary in height, width, and other geometric properties. Using both the first-order reliability method and polynomial chaos expansion, local and global sensitivity analysis is performed, providing insight into the most influential random variables as well as the influence of parameters related to monolith design. Sliding, overturning, and the CSO failure mode, introduced in Paper III, are evaluated and compared for two load cases that either consider ice load or an event in which the dam is overtopped. This study was designed and conducted, and the paper was written by the author of this thesis.

1.8 Additional Publications

In addition to the research papers appended to this thesis, the author has contributed to a journal paper and has published a Licentiate thesis and several conference papers. These publications are listed in this section but are not appended to the thesis.

Licentiate thesis

Ulfberg, A. (2023). A concrete dam assessment approach using probabilistic non-linear finite element analysis and scale model testing (Licentiate thesis). Luleå University of Technology.

Journal paper

Engineering Failure Analysis, 2021

Enzell, J., **Ulfberg, A.**, Sas, G., & Malm, R. (2021). Post-peak behavior of concrete dams based on nonlinear finite element analyses. *Engineering Failure Analysis*, 130, 105778. Doi.org/10.1016/j.engfailanal.2021.105778

Conference papers

ESREL Conference, Angers 2021

Ulfberg, A., Seger, A., Bista, D., Westberg Wilde, M., Johansson, F., Das, O., & Sas, G. (2021). Influence of concrete's mechanical properties on the cracking of concrete dams. *ESREL2021: 31st European Safety and Reliability Conference*. Angers, France.

IABSE Conference, Prague 2022

Ulfberg, A., Gonzalez-Libreros, J., Das, O., Sas, G., Andersson, E., Bista, D., Arntsen, B., Seger, A. (2022). Influence of large-scale asperities on the stability of concrete dams. *IABSE Symposium Prague*. Prague, Czech Republic.

ICOLD Conference, Gothenburg 2023

Ulfberg, A., Gonzalez-Libreros, J., Das, O., Sas, G., Malm, R., Johansson, F., Westberg Wilde, M. (2023). On the applicability of scale model tests for concrete dams: A review. *ICOLD-CIGB 2023*. Gothenburg, Sweden.

Fib symposium, Istanbul 2023

Agredo Chávez, A., **Ulfberg, A**., Gonzalez-Libreros, J., Elfgren, L., Sas. G. (2023). Data Validation of Strain-Based Monitoring Systems in Low Temperature Conditions, Case Study: The Kalix Bridge. *fib Symposium Istanbul 2023*. Istanbul, Turkey.

Chapter 2

2. Literature review

2.1 Background

By impeding the natural flow of water for storage and flood prevention, dams are essential to the built environment. They also facilitate hydropower generation, which supplied about 17% of the world's global electricity generation (IEA, 2021), highlighting the importance of maximizing their service life and support the transition to net-zero emissions. However, given the potentially severe consequences of failure for certain dams, it is essential that efforts to maximize their operational life do not come at the expense of safety. Dam safety assessment commonly comprises extensive programs, including structural analysis, monitoring data, maintenance plans, and other related actions (Wieland & Mueller, 2009), and is governed by various regulatory rules and guidelines (CDA, 2013; FERC, 2016; IS, 2019; NVE, 2005; RIDAS, 2025) to ensure satisfactory and consistent safety levels. Regarding the structural analysis component of concrete dam safety assessments, regulatory rules often ensure that stability and safety requirements are met by imposing deterministic criteria on the equilibrium equations for forces and moments acting on the dam. These criteria are based on predefined notions of how concrete dams fail, known as failure modes, such as sliding and overturning, which correspond to failure due to horizontal displacement and rotation about the toe, respectively. Some regulatory rules and guidelines also impose limits on the allowable stress magnitudes in the dam and foundation, since exceeding these limits can precede overturning and may lead to increased loads (RIDAS, 2025).

Such failure mode assessments, which consider only equilibrium equations, treat sliding and overturning as independent. They also use cautious safety factors to indirectly account for deformations and compatibility conditions (USACE, 2005) and are generally regarded as conservative (Ruggeri et al., 2004). Current practices for assessing failure modes often overlook geometrical irregularities and large-scale asperities on interfaces where sliding failures could take place, despite evidence that these features change the failure behavior and can greatly enhance the load capacity of concrete dams (Saichi et al., 2019; Sas et al., 2021). These features can, however, be accounted for using alternative methods, such as scale model testing and FEA, which are not constrained by the same idealizations.

Scale model testing has historically been employed to assess the load capacity and behavior of concrete dams (Fumagalli, 1973; Harris & Travers, 2006), since properly designed scale models will replicate the behavior and load capacity of the full-scale structure. A primary shortcoming of scale model testing is the need to adhere as closely as possible to scaling laws, which define the ratios between model and prototype parameters, thereby introducing practical constraints such as geometric scale and material properties (Harris & Sabnis, 1999). These constraints result in scale models having to be designed thoughtfully and constructed with great care, making scale model testing a relatively time-consuming and potentially expensive analysis method. FEA does not suffer these drawbacks and may be employed to numerically simulate the behavior and load capacity of dams. However, while FEA is not limited to the same idealizations as failure mode assessment based on equilibrium equations, it still relies on idealizations, which relate not only to the model's geometry but also to aspects such as element types and boundary conditions. This is especially true for NLFEA, which introduce simplified constitutive models to approximate material nonlinearity and also exhibit increased mesh dependency (Choi & Kwak, 1990). These drawbacks of FEA make it appropriate to verify the results obtained from FEA with experimental tests or monitoring data, especially for dams whose failure could have considerable consequences. However, whether using scale model testing or FEA, the dam's behavior and load capacity can be assessed without restricting the analysis to independent motions such as sliding and overturning failure modes. FEA analyses, however, generally need to conform to the safety factor format imposed by the guidelines and therefore must be made to fail in sliding and overturning (Malm, 2016). This requirement limits their advantage and effectively makes FEA similar to assessments based on equilibrium equations. As such, the core of the problem lies in whether sliding and overturning failure modes are truly representative of the actual failure behavior, and whether their underlying assumptions remain valid for dams with large-scale asperities and geometrical variations along the rock-concrete interface.

The use of global safety factors is another potential shortcoming of current regulatory rules and guidelines, as they define only the ratios between stabilizing and destabilizing loads and moments and do not directly account for the probability of events that may lead to failure or uncertainties in parameters. Furthermore, expressed as deterministically assessed ratios, current safety factors for sliding and overturning failure modes indicate the uniform increase in load magnitudes required to cause failure, which may represent unrealistic load scenarios. Adherence to safety factors may yield a predictable probability of failure for a load scenario, provided that the safety factors are calibrated (Vrouwenvelder, Baker, & Faber, 2025), as in standards such as the Eurocodes (CEN, 2006). However, these factors are conditional on the cases used for their calibration, meaning that the targeted safety level will be reliably achieved only for structures and conditions similar to those considered during calibration. Dams are generally unique, as they are designed and constructed for specific locations and may have considerable differences in design, geological conditions, loads, and other factors. Consequently, dams with similar safety factors can exhibit considerable differences in their probability of failure (Westberg Wilde & Johansson, 2016b). Reliability analysis may resolve these issues by directly accounting for uncertainties and the probabilities of various events for the dam and its associated prerequisites, with the probability of failure as a direct output. As dam assessment also typically involves multiple sources of uncertainty, including heterogeneous construction materials and loads governed by natural processes and phenomena, the use of reliability analysis is likely warranted. Consequently, interest in risk and reliability analysis applied to dam engineering has increased and the field has become an active area of research (Hariri-Ardebili, 2018; Przemyslaw, 2021), and guidelines have emerged in an attempt to standardize the approach (Westberg Wilde & Johansson, 2016a). Reliability analysis has the potential to address limitations of deterministic approaches by considering both inherent uncertainties and those related to unique prerequisites for individual dams. Reliability analysis also overcomes the limitation of evaluating translational and rotational safety measures independently in FEA, as is common in current practice. Such independent evaluation can otherwise require artificial boundary conditions in FEA models to induce failures such as overturning. Consequently, the safety of a dam under unrestricted failure behavior can be assessed by combining FEA with reliability analysis, which are often linked through the use of metamodeling.

Metamodeling, also commonly referred to as surrogate modeling, is a technique in which a simplified, computationally efficient model is created to approximate the output of a more complex and computationally expensive model, such as an FEA. The construction and use of metamodels is a very active field of research (Soares do Amaral et al., 2022). Their application in reliability analysis arises from the need, depending on the method, for gradients or numerous model evaluations, which may not always be readily available or practical. Research on the implementation of reliability analysis combined with metamodels has begun to emerge in dam engineering, but it remains far from fully mature, and although reliability analysis for concrete dams has progressed, most studies still focus on gravity dams and seismic events (Hariri-Ardebili, 2018). Similarly, few studies focus on the sensitivity analysis of dams, which investigates how changes in input variables affect the safety of dams and identifies key parameters and considerations. Such knowledge would likely support efforts to extend the service life of existing dams by providing a basis for more informed decision-making, not only regarding potential risk mitigation strategies but also concerning necessary strengthening actions.

2.2 Analytical dam stability assessment methods

2.2.1 Sliding stability assessment

Sliding refers to failure caused by the dam, or parts of the dam, undergoing horizontal displacement. Assessing the sliding stability of a dam involves comparing the total shear resistance, R, of the interfaces with the total shearing forces, ΣH, acting on them. A generalized model of R for an interface can be expressed through the local shear capacity (Altarejos-García, Escuder-Bueno, & Morales-Torres, 2015), given by a shear strength criterion dependent on the local normal stress and integrated over the interface, as shown in Eq. (2.1).

$$R = \int_S \tau_\mathrm{f}\left(\sigma_n\left(x,y\right)\right)\mathrm{d}A \tag{2.1}$$

where $\tau_\mathrm{f}(\sigma_n(x,y))$ denotes the local shear strength as a function of the normal stress at a point on the interface, and S denotes the interface surface. Under a rigid body assumption, or assuming uniform stresses and constant values for all other parameters influencing shear strength, the total shear strength of the interface reduces to the product of the shear strength criterion, now constant over the whole interface, and the interface area, as shown in Eq. (2.2).

$$\tau_\mathrm{f}\left(\sigma_n\left(x,y\right)\right) = \tau_\mathrm{f}\left(\sigma_n\right) \rightarrow R = \tau_\mathrm{f}\left(\sigma_n\right)\int_S \mathrm{d}A = \tau_\mathrm{f}\left(\sigma_n\right)A \tag{2.2}$$

where A denotes the total area of the interface. Eq. (2.2) may be further simplified by employing the Mohr-Coulomb failure criterion, as is commonly done in practice (Nicholson, 1983; USACE, 2005), to obtain Eq. (2.3).

$$\tau_\mathrm{f}\left(\sigma_n\right) = c + \sigma_n \tan\left(\phi\right) \rightarrow R = \left(c + \sigma_n \tan\left(\phi\right)\right)A = cA + N\tan\left(\phi\right) = cA + N\mu \tag{2.3}$$

where c denotes cohesion (assumed to be constant), ϕ denotes the friction angle, N denotes the sum of normal forces over the interface, and $\mu = \tan(\phi)$ denotes the coefficient of friction. Three methods to assess safety against sliding are generally provided by guidelines and regulatory rules: namely the *sliding resistance method* (Eq. (2.4)), the *shear friction method* (Eq. (2.5)), and the *limit equilibrium method* (LEM) (Eq. (2.6)) (Johansson, 2009).

$$\mu = \frac{\sum H}{\sum V'} \leq \mu_\mathrm{allowable} \tag{2.4}$$

$$SF = \frac{cA + \sum V'\tan\left(\phi\right)}{\sum H} \geq SF_\mathrm{min} \tag{2.5}$$

$$SF = \frac{\tau_f(\sigma_n)}{\tau} \geq SF_{\min} \tag{2.6}$$

where μ denotes the friction angle required for force equilibrium, based on the sum of effective vertical forces $\Sigma V'$ (i.e., N) and sum of horizontal forces ΣH, $\mu_{\text{allowable}}$ denotes the maximum allowable friction angle specified by the guideline, SF denotes the corresponding safety factor, $SF_{\min}$ denotes the minimum allowed safety factor by the guideline, and τ denotes the shear stress. Any failure criterion can in principle be employed for LEM, but the Mohr-Coulomb failure criterion is most often assumed (USACE, 2005). Consequently, the shear friction method and LEM are effectively identical, as indicated by the relationships in Eqs. (2.2)-(2.3). Furthermore, if cohesion is neglected, all three methods effectively provide identical results and differ only in how they represent safety. In LEM, which is the most common (Soltani, Escuder-Bueno, & Klun, 2024), and in the shear friction method, safety is represented by the ratio of resisting forces to driving forces, whereas in the sliding resistance method, used in Sweden and Italy (Krounis, 2016), safety is expressed as the inverse ratio, with the shear strength criterion omitted.

It is important to note the significance of assuming either constant stresses or rigid-body motion for the validity and accuracy of all the methods, as local exceedance of the shear strength may lead to progressive failure along the interface. Although dams are considerably stiff, they are not rigid. Furthermore, when potential stress redistributions during construction, features such as inspection galleries, uplift, material heterogeneity, possible shear deformation, and eccentric loading are taken into account, the assumption of constant stress along the interface is unlikely to be entirely accurate. Consequently, localized failures may occur along dam interfaces, resulting in displacements and stress redistribution, as acknowledged in other studies (Pereira et al., 2022). Evidence of such phenomena has been observed in scale model tests of a gravity dam with a jointed foundation (Lemos et al., 1995) in which the ultimate capacity was obtained only after the model had undergone displacements, indicating stress redistribution and changing equilibrium conditions. These phenomena have also been observed in studies of rock-concrete interfaces in dams with geometrical irregularities and large-scale asperities, where stresses concentrate at the asperities and steeply inclined portions of the interface (Saichi & Bouaanani, 2024; Saichi et al., 2019; Sas et al., 2021). In these studies, the horizontal load capacity was considerably greater than that predicted by sliding assessments, indicating that Eqs. (2.4)-(2.6) may be inadequate and could underestimate the load capacity of dams when interfaces are not completely plane.

2.2.2 Overturning stability assessment

Overturning refers to failure by toppling of the dam and occurs when the stabilizing moments, ΣM_{S}, are equal to or less than the destabilizing moments, ΣM_{DS}. In the analysis of overturning, the dam is assumed to rotate about the toe, and the safety against overturning is commonly expressed mathematically as Eq. (2.7) (NVE, 2005; RIDAS, 2025).

$$SF = \frac{\sum M_{\mathrm{S}}}{\sum M_{\mathrm{DS}}} > SF_{\min} \tag{2.7}$$

The implementation and requirements for assessing the overturning failure mode vary across guidelines and regulatory rules, as idealized overturning would imply infinite stress magnitudes at the toe, which, in reality, would be preceded by crushing of the dam toe (CFGB, 2002). In cases where guidelines and regulatory rules omit overturning, the tendency of a dam to rotate is instead commonly evaluated by assessing stresses along the interfaces.

2.2.3 Core boundary and overstressing

The core boundary refers to the region of the dam's cross-section through which the resultant of all external forces must pass to ensure that no tensile stresses develop anywhere along the rock-concrete interface. The core boundary concept is illustrated in Figure 2, where ΣM and ΣV denote the sum of moments about the neutral axis and the sum of vertical loads, respectively. Provided that the resultant remains within the core boundary, the interface experiences only compressive stresses. Since overturning occurs when the resultant's line of action intersects the foundation outside the dam's base, keeping the resultant within the core boundary prevents overturning. In some guidelines and regulatory rules, evaluation of the core boundary is used as a criterion instead of explicitly checking for overturning (CFGB, 2002; USACE, 2005), while in others, both approaches are applied (RIDAS, 2025). The justification for applying both approaches lies in the concern over tensile stresses in the interface, as these can cause separation or cracking, which in turn may increase the uplift pressure (Westberg Wilde & Johansson, 2016a). However, the actual consequences of tensile stresses in the interface are difficult to determine because the interface may possess some cohesion and tensile strength, and separation or cracking in the interface may not imply global failure of the dam.

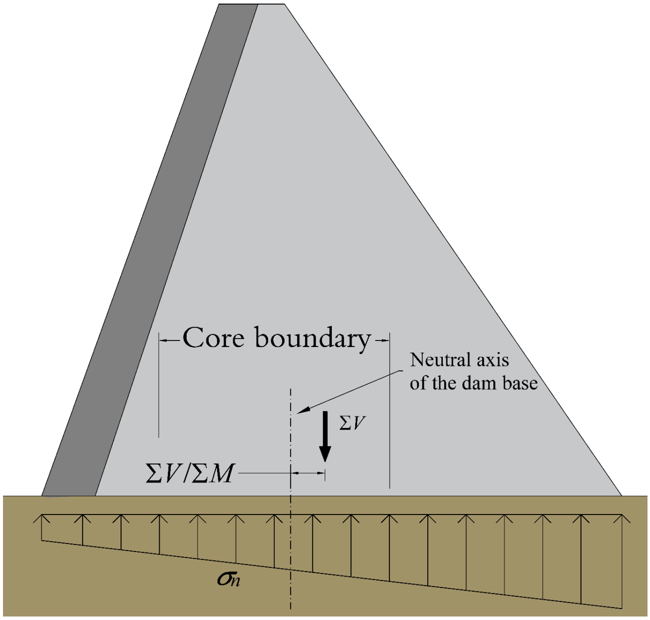

Figure 2. Core boundary for a buttress dam.

Due to the nature of the loading on dams, tensile stresses mainly concern the dam heel, which generally experiences the lowest compressive stresses, whereas the toe experiences the greatest. Consequently, the dam toe is commonly evaluated for overstressing with respect to compressive stresses to ensure they do not exceed the allowable levels specified by the relevant design guidelines or standards. These stresses may be calculated using Navier's formula (Eq. (2.8)) (CFGB, 2002).

$$\sigma_x = \frac{N}{A} \pm \frac{xM_c}{I} \tag{2.8}$$

where σ_x denotes the stress at a distance x from the neutral axis of the dam base cross-section, M_c denotes the moment about the neutral axis of the dam base cross-section, and I denotes the moment of inertia of the dam base cross-section. In contrast to the assumptions made for sliding, when assessing stresses in the interface, the distribution is no longer assumed to be constant and is instead assumed to be linear according to Bernoulli's hypothesis, although this assumption is not entirely accurate for dams (Reinius, 1962). However, if a more refined analysis is required, FEA may be employed (USACE, 1995).

2.2.4 Limit turning

Limit turning is a failure mechanism that begins with tensile cracks in the foundation, followed by rotation of the dam (Fishman, 1979), and stems from observed discrepancies between the sliding failure mode and experimental shear tests on concrete blocks cast on rock foundations. The tensile cracks initiate at the dam's heel and propagate through the foundation in a parabolic shape, oriented perpendicular to the direction of the principal maximum stresses, toward the toe for increasing loads. As the compressed zone progressively shrinks, it eventually undergoes crushing failure, and the ultimate capacity is reached (Fishman, 1988). The load capacity of a dam for the limit turning failure mode may be evaluated using Eq. (2.9) (Fishman, 2008).

$$T_{\mathrm{p}} = \sqrt{2NetR_{cr} + \left(htR_{cr}\right)^2 - N^2} - htR_{cr} \tag{2.9}$$

where N denotes the sum of vertical loads, e and h denote the lever arms for the vertical and horizontal load sums, respectively, t denotes the width of the dam section, and R_{cr} denotes the crushing resistance of the rock. To the author's knowledge, limit turning is not implemented in any guidelines and, while certainly a valid failure mechanism, may only be relevant under certain conditions. As limit turning develops and progresses due to considerable tensile forces in the foundation, which cause the rock to crack, tensile forces of similar magnitude must first traverse the interface. This implies that the tensile strength of the interface must be comparable to that of the surrounding rock in the foundation and the concrete. Furthermore, for dams with relatively small base areas, such as buttress dams, the combined tensile strength of the concrete at the dam base is likely considerably smaller than that of the foundation, provided that the rock mass is not heavily jointed. The limit turning failure mechanism has, however, been experimentally produced for unbonded bodies in contact, but the only instances in which a limit turning failure occurred were in a few models consisting of small metal blocks on gypsum (Fishman, 2008).

2.3 Scale model testing

Historically, scale model testing has been used to assess the load capacity and stability of dams, with prominent laboratories such as the Istituto Sperimentale Modelli e Strutture (ISMES) (Fumagalli, 1973) and the Laboratório Nacional de Engenharia Civil (LNEC) (Lemos et al., 1995; Oliveira & Faria, 2006) employing this analysis technique. However, numerical analysis methods such as FEA are now more common (Malm, 2016) due to their significant improvement and widespread implementation in civil engineering. Despite this, experimental testing still serves an important verification purpose and scale model testing continues to be used to assess dams' load capacities, mainly in China (Liu et al., 2003; Liu et al., 2020; Liu et al., 2013; Yang et al., 2015; Zhang et al., 2004; Zhang et al., 2019). Recently, scale model testing has been actively used to study the effects of underwater explosions on concrete dams (Gao et al., 2025; Huang, 2024; Jiang et al., 2025; Li, Lei, & Huang, 2024; Liu et al., 2025; Wu, Chen, & Cheng, 2025; Xiong et al., 2024).

Scale model testing simplifies experiments by allowing a problem to be modeled, in theory, at any scale, while still capturing the behavior of the real structure, commonly referred to as the *prototype*. This is due to the fact that natural phenomena depend only on the relationships between fundamental quantities and are independent of the units used. However, for a scale model to mimic the behavior of the prototype, it must remain in *similitude*. Similitude implies that the relationships between corresponding physical quantities in the scale model and the prototype are maintained according to defined scaling laws (Sonin, 2001). Scaling laws define the ratios between parameters' magnitudes in the prototype and in the scale model, commonly referred to as scale factors and defined by Eq. (2.10).

$$S_X = \frac{X_\mathrm{P}}{X_\mathrm{M}} \tag{2.10}$$

where S_X denote the scale factor for a parameter X, and subscripts P and M denote the parameters value in the prototype and the scale model, respectively. Parameters with the same units will have identical scale factors, as these are determined by the fundamental dimensions rather than the units themselves (Harris & Sabnis, 1999). Scale models used to study phenomena in concrete structures subjected to static loads commonly follow one of two scaling laws. One aims to maintain similar stress magnitudes in the scale model and prototype and is hereafter referred to as "stress-fixed scaling", while the other aims to maintain similar material densities and is hereafter referred to as "density-fixed scaling". Both scaling laws are defined by Eq. (2.11), which expresses the scale factors in terms of units that encompass most parameters relevant for static scale model tests on concrete structures.

$$S_{[\mathrm{m}]}S_{[\mathrm{N/m^3}]} = S_{[\mathrm{N/m^2}]} = \frac{S_{[\mathrm{N/m}]}}{S_{[\mathrm{m}]}} = \frac{S_{[\mathrm{N}]}}{S^2_{[\mathrm{m}]}} \tag{2.11}$$

All expressions in Eq. (2.11) must be identical, and determining a scaling law for static tests on concrete structures involves selecting values for two of the scale factors and solving for the remaining factors. Scale factors for dimensionless parameters must be equal to one. Based on their compliance with the scaling laws, models can be classified into three categories (Harris & Sabnis, 1999): *true models*, *adequate models*, and *distorted models*. A true model fully adheres to the scaling laws and produces results identical to those of the prototype, whereas a distorted model fails to comply with one or more important scaling laws, potentially yielding results that deviate from the prototype. An adequate model exhibits some distortions with respect to the scaling laws but complies for the parameters that govern the phenomenon under study, thereby producing results and behaviors consistent with the prototype. An example of a distorted model is given by (Allen et al., 1956), where rubber was used to emulate concrete, resulting in inaccurate displacements due to distortions in properties such as Poisson's ratio and the stress-strain relationship. Another distortion that, to the author's best knowledge, is present in all scale model tests on concrete structures, yet seldomly acknowledged, is the scaling of fracture energy. Eq. (2.11) states that fracture energy, expressed in units of [N/m], must be scaled differently from parameters expressed in units of [N/m^2], such as tensile strength, with which it is known to correlate (Modéer, 1979). This distortion likely introduces size effects (Bažant, 1984), as shown in experiments on crack-mouth opening displacements of gravity dams (Barpi & Valente, 2000), where the load capacity of identical models increased as their size decreased. Naturally, the influence of this distortion depends on the scale model's behavior and failure, as well as on the phenomena under study.

In practice, it is therefore impossible to produce a scale model of a concrete structure that is entirely free of distortions. However, distortions can be mitigated through careful design and construction and through thoughtful selection of scaling laws, which have practical implications for experimental testing (Ulfberg et al., 2023). In stress-fixed scaling, where $S_{[N/m^2]} = 1$ in Eq. (2.11), the main practical implication is that the density of the scale model materials, governed by $S_{[N/m^3]}$, becomes inversely proportional to the geometric scale of the model, determined by $S_{[m]}$. Consequently, while material properties expressed in [N/m^2], such as compressive strength, tensile strength, and modulus of elasticity, should remain the same between the scale model and the prototype, the density of the scale model material must be greater, provided that the model is smaller than the prototype. Because few suitable aggregates exist to increase the density sufficiently to allow a geometric scale smaller than 1:2 for a scale model (Fumagalli, 1973), this density increase is generally simulated artificially for smaller scales. Examples of approaches to supplement the additional mass for similitude include the use of hanging weights (Barpi et al., 1998) or tendons embedded in the scale model and tensioned prior to testing (Oberti & Fumagalli, 1979). Scale model tests in centrifuges have also been used (Plizzari, Waggoner, & Saouma, 1995). Considering that centrifugal acceleration increases with distance from the axis of rotation, a potential drawback of using a centrifuge is that an uneven increase in effective gravity (and hence density) can occur, which is exacerbated when the scale model occupies a large portion of the centrifuge radius.

In density-fixed scaling, where $S_{[N/m^3]} = 1$ in Eq. (2.11), the main practical implication is that the material properties expressed in $S_{[N/m^2]}$ become proportional to the geometric scale of the model, determined by $S_{[m]}$. As a result, parameters such as the modulus of elasticity, compressive strength, and yield stress of reinforcement for the scale model's materials need to be reduced, whereas in stress-fixed scaling, similar materials can be used in the scale model as in the prototype. Including reinforcement steel in scale models of a density-fixed scaling type will therefore introduce distortions, and due to the lack of alloys that mimic the stress-strain behavior of reinforcement steel, reinforcement is usually omitted for such models. Naturally, this is only viable for dams where reinforcement has little influence on the behavior and load capacity and is most often implemented in scale models of large gravity dams (Chen et al., 2012) or arch dams (Chen et al., 2015) with considerable geometric downscaling. To facilitate downscaling of the scale model material to follow similitude, the mix used to emulate the dam concrete is typically based on gypsum or cement mortar and is intentionally weakened with additives such as oil or wax (Stimpson, 1970). This type of scaling law is also often used for so-called geomechanical models (Fumagalli, 1966), which are essentially scale models that place greater emphasis on the dam foundation and often include features such as faults and persistent rock joints as in (Fei, Zhang, & Zhang, 2010; Liu et al., 2013).

Such considerations and the necessity for rigorous design and construction limit the applicability of scale model testing. However, data obtained from scale model tests have proven valuable and have been used in the assessment of several well-known dams, such as the Jinping I arch dam (Chen et al., 2015; Fei, Zhang, & Zhang, 2010; Yang et al., 2015) and the Three Gorges dam (Liu et al., 2003).

2.4 Finite element analysis

FEA enables numerical simulation of complex structural behavior under various loads, such as seismic events and temperature effects, where analytical approaches may have limited applicability. Although not explicitly prescribed by regulatory rules and guidelines as an assessment method, it is commonly used in dam engineering to design and optimize both new dams and remedial works (ICOLD, 2013). Nonlinear FEA (NLFEA) can capture material nonlinearities, cracking, and joint interactions, providing a detailed understanding of stress, strain, and deformation throughout the dam. As such, internal failure modes of concrete dams and foundation failure may be assessed (Enzell, 2023). However, from a global stability perspective, when a dam is assessed for sliding or overturning stability, FEA might be unnecessary if the dam is expected to behave as a monolithic structure without cracks that could lead to internal failure modes (Malm, 2016). This is due to the analysis potentially having to be made compliant with the safety factor format (Enzell et al., 2021), which may require the use of artificial boundary conditions to enforce an overturning failure mode. In addition, the rock-concrete interface may need to be modeled as entirely flat to obtain a sliding failure mode. For such cases, FEA is likely to provide results identical to those obtained from analytical assessment of sliding and overturning (Fu & Hafliðason, 2015), as FEA is effectively used as a simulation of force and moment equilibrium. This is not an inherent drawback of FEA, but rather a consequence of prescribing specific failure mode analyses, restricting its potential for global stability assessment.

2.5 Reliability and sensitivity analysis

2.5.1 Fundamentals and application to dams

Reliability analysis concerns the evaluation of the probability that a structure or component will fail to fulfill its design purpose over a specified design lifetime (Nowak & Collins, 2013). This probability is referred to as the *probability of failure*, P_f, with *reliability* defined as its complement (Mencik, 2016). The reliability of a structure depends on the performance function, which describes the structural behavior being evaluated, and on the random variables $\mathbf{X} = [X_1, X_2, \ldots, X_n]^T$ associated with the problem. Random variables are stochastic variables that, in contrast to deterministic variables described by a single value, are characterized by a probability distribution. They reflect uncertainty in aspects such as loads and material properties, which influence the resistance or capacity R of the structure or component, as well as the demand or load action S. Using such a framework, and if the resistance and the demand are separable, the performance of a structure can be described as in Eq. (2.12), which is commonly referred to as the limit state function (LSF).

$$G(\mathbf{X}) = R(\mathbf{X}) - S(\mathbf{X}) \tag{2.12}$$

Using this formulation, failure of the structure or component is indicated by negative values of G, whereas positive values indicate that it is performing as intended. The probability of failure for the structure or component is then given by the integral over the failure domain (Lemaire, Chateauneuf, & Mitteau, 2013), as defined in Eq. (2.13).

$$P_f = P\left[G(\mathbf{X}) \leq 0\right] = \int_{G(\mathbf{X}) \leq 0} f_{\mathbf{X}}(\mathbf{x})\,\mathrm{d}\mathbf{x} \tag{2.13}$$

where P[·] denotes the probability of the event, and $f_{\mathbf{X}}(\mathbf{x})$ denotes the joint probability density function (PDF) of $\mathbf{X}$. The integral in Eq. (2.13) represents an n-fold integral of the joint PDF of the random variables over the failure domain, and solving this integral is one of the most difficult problems in reliability analysis (Der Kiureghian, 2022). Consequently, significant research efforts have been devoted to develop methods to approximate the integral in Eq. (2.13), such as simulation-based methods, which operate via numerical integration, and the first- and second-order reliability methods (FORM and SORM), which use first- and second-order Taylor expansions of the LSF, respectively (Nikolaidis, Ghiocel, & Singhal, 2004).

Although versatile, these methods suffer from limitations related to the LSF function. Conducting FORM and SORM requires the gradient and Hessian of the LSF, respectively, which limits their application to problems where these derivatives with respect to the random variables are readily available. Although robust by guaranteeing convergence to the probability of failure (Song & Kawai, 2023), simulation-based methods are computationally expensive, often requiring thousands to millions of simulations depending on the probability of failure and the chosen simulation method. Consequently, they are ill-suited for direct application to problems using NLFEA as the LSF, since the gradient is difficult to obtain and performing thousands of simulations is impractical. To address these shortcomings, the use of metamodels, which are less computationally expensive black-box functions that approximate the output of the function they are intended to surrogate, has become increasingly popular in reliability analysis (Ellingwood et al., 2025). Today, multiple approaches and methods exist for constructing metamodels, including the *response surface method* (RSM) (Khuri & Mukhopadhyay, 2010), *polynomial chaos expansion* (PCE) (Sudret, 2014), *Kriging* (Echard, Gayton, & Lemaire, 2011), and *polynomial chaos-Kriging* (PC-Kriging) (Schöbi, 2017). Such approaches may be used to surrogate a more complex LSF and can be used in combination with FORM, SORM, or simulation-based methods to determine the reliability.

Unlike deterministic analysis, reliability analysis considers uncertainties in the structure or its components, offering a more nuanced, case-specific evaluation of structural safety. Although guidelines for its application to dams have been proposed (Westberg Wilde & Johansson, 2016a) and interest in risk-based assessments in dam engineering is growing (Przemyslaw, 2021), the practical implementation of reliability analysis has remained slow (Altarejos-García, Escuder-Bueno, & Morales-Torres, 2015). An important benefit of using reliability analysis, aside from its ability to account for uncertainties, is that it can be applied to any failure mode and any type of failure behavior observed in, for example, FEA, thereby circumventing safety factors that are tied to specific failure modes. Consequently, the probability of failure for a mode that is neither sliding nor overturning can be assessed, and using it in combination with analysis methods such as FEA may eliminate the need for idealizations and artificial boundary conditions to force a specific failure mode.

Apart from assessing the reliability of a structure, it is often crucial to understand the influence of individual parameters on the probability of failure (Saltelli & Annoni, 2010). Sensitivity analysis provides such insight by quantifying how variations in random variables affect reliability, often through the calculation of various sensitivity measures such as partial derivatives of the LSF (Patil & Frey, 2004), omission sensitivity factors (Madsen, 1988), Sobol' indices (Sobol', 1993), or moment independent indices (Borgonovo, 2007; Iman & Hora, 1990). By identifying the parameters with the greatest impact, sensitivity analysis not only guides the prioritization of data collection and refinement of calculation models (Saltelli et al., 2008) but also informs design decisions and mitigation strategies.

Sensitivity analysis has been applied to concrete dams, including studies on the influence of variables in concrete gravity dams during seismic events (Hussein et al., 2025), parameters related to rock joints in a concrete arch dam (Ahmadi & Soltani, 2021), and rock and concrete parameters during the impoundment of an arch dam (Khaneghahi, Alembagheri, & Soltani, 2019), among others (Altarejos-García et al., 2012; Li, 2021; Su et al., 2016; Xu & Wang, 2023). However, existing studies tend to focus on gravity or arch dams under seismic events and on specific case studies of particular dams, which may limit the generalizability of the results, and only a few (De Sortis & Paoliani, 2007; Muda et al., 2024) consider buttress dams.

2.5.2 FORM, SORM, and simulation-based methods

FORM is a gradient-based approach that uses a first-order Taylor series expansion (i.e., a linear approximation) of the limit-state function at the most probable failure point (MPFP or MPP), commonly denoted as $\mathbf{u}^{*}$, which is the point on the failure surface $G(\mathbf{X})=0$ with the highest probability density (Nowak & Collins, 2013). This point lies in the standard normal space, often referred to as u-space, which is defined by the set of statistically independent standard normal random variables $\mathbf{U} = [U_1, U_2, \ldots, U_n]^{\mathrm{T}}$ (Choi, Grandhi, & Canfield, 2007). The MPFP is also the point on $G(\mathbf{X})=0$ that is closest to the origin of the standard normal space, and this Euclidean distance, denoted β, is referred to as the *reliability index* (Huang, El Hami, & Radi, 2017a). The standard normal space and the original space of the random variables, commonly referred to as x-space, are related through an isoprobabilistic transformation of the random variables (Lemaire, Chateauneuf, & Mitteau, 2013). This transformation can be performed using several approaches, such as the equivalent normal distribution transformation (Nowak & Collins, 2013), the Nataf transformation (Nataf, 1962), the Rosenblatt transformation (Rosenblatt, 1952), or copula functions (Nelsen, 2006). The LSF may be expressed as a function of $\mathbf{U}$, as in Eq. (2.14), granted that the cumulative distribution functions (CDFs) of the random variables in the original space are continuous and not constant over any range (Der Kiureghian, 2022).

$$G(\mathbf{U}) = G\left(\mathrm{T}(\mathbf{X})\right) \tag{2.14}$$

where $\mathrm{T}(\cdot)$ denotes the transformation function. The linearized LSF at the MPFP may then be written as in Eq. (2.15) at the MPFP (Nikolaidis, Ghiocel, & Singhal, 2004).

$$G(\mathbf{U}) = G\left(\mathbf{u}^{*}\right) + \nabla G\left(\mathbf{u}^{*}\right)\left(\mathbf{U} - \mathbf{u}^{*}\right) = \left\|\nabla G\left(\mathbf{u}^{*}\right)\right\|\left(\beta - \hat{\boldsymbol{\alpha}}\mathbf{U}\right) \propto \beta - \hat{\boldsymbol{\alpha}}\mathbf{U} \tag{2.15}$$

where $\nabla G(\mathbf{u}^*)$ is the gradient vector at the MPFP, and $\hat{\boldsymbol{\alpha}}$ is the negative normalized gradient vector at the MPFP, as defined in Eq. (2.16).

$$\hat{\boldsymbol{\alpha}} = -\frac{\nabla G\left(\mathbf{u}^*\right)}{\left\|\nabla G\left(\mathbf{u}^*\right)\right\|} = \frac{\mathbf{u}^*}{\beta} \tag{2.16}$$

Because the standard normal space is rotationally symmetric and the random variables are independent with a joint multivariate standard normal PDF, $\phi_n(\mathbf{u})$, the integral in Eq. (2.13) reduces to Eq. (2.17).

$$P_f \approx \int_{\beta-\hat{\boldsymbol{\alpha}}\mathbf{u}\le 0} \phi_n\left(\mathbf{u}\right)\, \mathrm{d}\mathbf{u} = \Phi\left(-\beta\right) \tag{2.17}$$

where $\Phi(\cdot)$ is the standard normal CDF. Consequently, the FORM approximation of the probability of failure is the distance β from the origin in the standard normal space to the MPFP, as graphically illustrated in Figure 3.

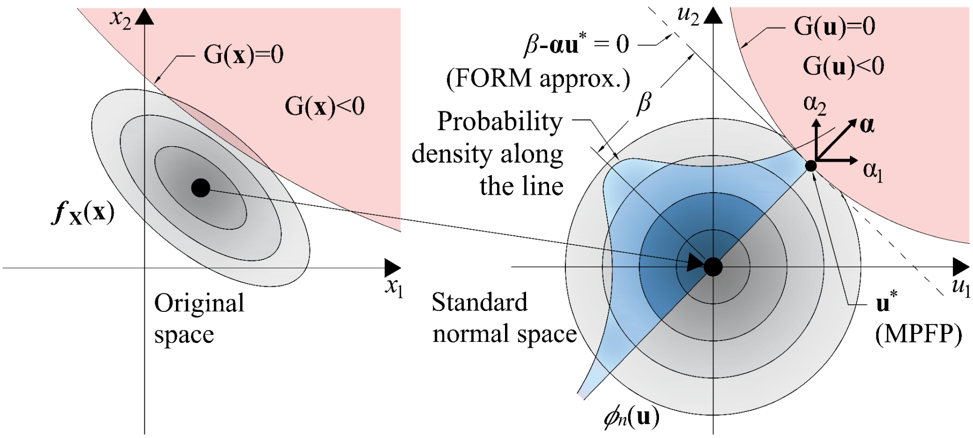

Figure 3. Reliability problem and FORM approximation for two random variables shown in both the original space and the standard normal space.

The main effort in FORM is finding the MPFP, which is a constrained optimization problem (Nikolaidis, Ghiocel, & Singhal, 2004) for which several algorithms and methods have been developed. One of the first algorithms is the HLRF (Hasofer-Lind Rackwitz-Fiessler) algorithm (Rackwitz & Fiessler, 1978) which converges quickly. Although popular, the HLRF algorithm has difficulties converging for highly nonlinear problems (Roudak et al., 2017). Recognizing this shortcoming, the iHLRF algorithm (Zhang & Der Kiureghian, 1994) modifies the original algorithm by introducing a merit function to control the step length, resulting in unconditional convergence to the MPFP (Sudret & Der Kiureghian, 2000). A differentiable merit function for the HLRF algorithm has also been proposed (Regina, Matioli, & Beck, 2012), which enables verification that a sufficient reduction in the merit function is achieved. Other algorithms have been proposed that incorporate chaos control (Yang, 2010), the Broyden-Fletcher-Goldfarb-Shanno algorithm (Periçaro et al., 2015), and particle swarm optimization algorithms (Zhu et al., 2022).

One of the weaknesses of FORM is its linear approximation, which results in probability of failure estimates being exact only for LSFs that are linear in the standard normal space. The nonlinearity of the LSF arises not only from the original function but also from the transformation from the original space to standard normal space (Lemaire, Chateauneuf, & Mitteau, 2013). This implies that LSFs that are linear in the original space may be nonlinear in the standard normal space if the original distributions have a nonlinear mapping to the normal distribution. SORM mitigates this issue of nonlinearity by using the second-order Taylor series expansion at the MPFP. However, because the probability content of the region beyond the second-order approximation is difficult to assess, SORM methods generally use an approximation (Mansour, 2016), expressed in terms of the principal curvatures of a paraboloid with its vertex at the MPFP, as in Eq. (2.18).

$$\tilde{G}\left(\tilde{\mathbf{u}}\right) \approx \beta - \tilde{u}_n + \frac{1}{2}\sum_{i=1}^{n-1} \kappa_i \tilde{u}_i^2 \tag{2.18}$$

where $\tilde{G}$ denotes the LSF scaled by the norm of the gradient, $\tilde{u}$ denotes u in a rotated coordinate system such that one of the random variables aligns with the negative normalized gradient vector, and κ_i are the principal curvatures of the paraboloid. In this format, several approximations for the parabolic domain in Eq. (2.18) have been proposed, such as Eq. (2.19) (Breitung, 1984), Eq. (2.20) (Hohenbichler & Rackwitz, 1988), and Eq. (2.21) (Tvedt, 1990).

$$P_f \approx \Phi\left(-\beta\right) \prod_{i=1}^{n-1} \frac{1}{\sqrt{1+\beta\kappa_i}} \tag{2.19}$$

$$P_f \approx \Phi\left(-\beta\right) \prod_{i=1}^{n-1} \frac{1}{\sqrt{1+\kappa_i\, \phi\left(\beta\right) / \Phi\left(-\beta\right)}} \tag{2.20}$$

$$P_f \approx \phi\left(\beta\right) \mathrm{Re}\left\{ \mathrm{i}\sqrt{\frac{2}{\pi}} \int_0^{\mathrm{i}\infty} \frac{1}{s} \exp\left[\frac{\left(s+\beta\right)^2}{2}\right] \prod_{i=1}^{n-1} \frac{1}{\sqrt{1+\kappa_i s}}\, \mathrm{d}s \right\} \tag{2.21}$$

where $\phi(\cdot)$ denotes the standard normal univariate PDF. As such, the SORM approximation essentially becomes the FORM approximation with correction factors to account for the curvature of the LSF. For these SORM estimates, the inequality $-1<\beta\kappa_i$ must hold for all principal curvatures (Der Kiureghian, 2022) since the curvatures cannot extend beyond a circle of radius β around the origin, otherwise the MPFP obtained from

FORM would be incorrect. Although SORM is generally more accurate than FORM, it is seldom exact, and it is also more computationally expensive because the Hessian is needed to compute the principal curvatures (Hurtado, 2013). An approximation for the principal curvatures, shown in Eq. (2.22), has been developed (Der Kiureghian & De Stefano, 1991) that, instead of the Hessian, uses the negative normalized gradient vector and the design point (i.e., a candidate in the MPFP search) from the last two iterations.

$$\kappa_i \approx \frac{\operatorname{sgn}\left[\hat{\boldsymbol{\alpha}}_r\left(\mathbf{u}_r-\mathbf{u}_{r-1}\right)\right]\cos^{-1}\left(\hat{\boldsymbol{\alpha}}_{r-1}\hat{\boldsymbol{\alpha}}_r^{\mathrm{T}}\right)}{\sqrt{\left\|\mathbf{u}_r-\mathbf{u}_{r-1}\right\|^2-\left[\hat{\boldsymbol{\alpha}}_r\left(\mathbf{u}_r-\mathbf{u}_{r-1}\right)\right]^2}} \tag{2.22}$$

where $\hat{\boldsymbol{\alpha}}_r$ and $\hat{\boldsymbol{\alpha}}_{r-1}$ are the negative normalized gradient vectors for the last and second-to-last FORM iterations, respectively, and $\mathbf{u}_r$ and $\mathbf{u}_{r-1}$ are the design points for the last and second-to-last FORM iterations, respectively. Recent developments in SORM include methods based on the asymptotic expansion of the distribution of a linear combination of noncentral chi-squared variables (Mansour & Olsson, 2014), differential geometry (Ferreira et al., 2019), and spherical integration (Chen et al., 2024).

Simulation-based methods, generally referred to as Monte Carlo simulation (MCS), do not suffer from the limitation of having an inherent accuracy bound for each problem, unlike FORM and SORM, where the accuracy is limited by how well the LSF resembles a first- or second-order expansion. Simulation-based methods rely on numerical integration, performed by evaluating numerous samples of $G(\mathbf{X})$, and employ an indicator function that outputs 1 if $G(\mathbf{X})\leq 0$ and 0 if $G(\mathbf{X})>0$. In its most basic form, where sampling is performed randomly across the entire input space, commonly referred to as crude MCS, Eq. (2.13) simplifies to Eq. (2.23) (Melchers & Beck, 2018).

$$P_f = \int_{-\infty}^{\infty} I\left[G(\mathbf{x})\leq 0\right] f_{\mathbf{X}}(\mathbf{x})\,\mathrm{d}\mathbf{x} \approx \frac{1}{N}\sum_{i=1}^{N} I\left[G(\mathbf{x}_i)\leq 0\right] = \frac{N_f}{N} \tag{2.23}$$

where $I(\cdot)$ denotes the indicator function, N denotes the number of samples, N_f denotes the number of samples where $G(\mathbf{X})\leq 0$. While MCS is easy to implement, can be applied to almost all reliability problems, and allows the probability of failure to be estimated to any desired accuracy (Huang, El Hami, & Radi, 2017b), its biggest drawback is the reliance on a considerable number of evaluations of the LSF. This has led to the development of variance reduction techniques (Bjerager, 1990), which aim to reduce the variance of the indicator function, thereby improving the method's efficiency and allowing for fewer LSF evaluations. These include methods based on, or incorporating, importance sampling (Harbitz, 1986), subset simulation (Au & Beck, 2001), directional simulation (Bjerager, 1988), line sampling (Koutsourelakis, Pradlwarter, & Schuëller, 2004), Latin hypercube sampling (LHS) (McKay, Beckman, & Conover, 1979), quasi-

Monte Carlo (QMC) sampling (Faure, 1981; Halton, 1960; Sobol', 1967), and antithetic variates (Schuëller et al., 1989). Sampling-based methods continue to attract attention and remain popular due to their versatility, and many new approaches building on these methods continue to be developed (Song & Kawai, 2023).

2.5.3 Metamodeling

The concept of metamodeling is to generate a simpler and more computationally efficient model than the function that the metamodel seeks to replicate. Although not true for all types of metamodels, metamodeling can be crudely viewed as a specialized form of regression. Its use in structural reliability is relatively recent, with the first applications in combination with FEA (Faravelli, 1989). Since then, metamodeling has received considerable research interest, and many different approaches to construct a metamodel have been developed (Roy & Chakraborty, 2023; Saraygord Afshari et al., 2022; Teixeira, Nogal, & O'Connor, 2021; Xu & Saleh, 2021). While their approaches differ on how to construct a so-called surrogate function, they all share the need for calibration, commonly referred to as training (Huang, El Hami, & Radi, 2017c). Training involves calibrating the metamodel using input-output pairs from the original function so that the metamodel produces outputs that accurately represent the original function for inputs not included in the training set. The accuracy of a metamodel is usually assessed through error estimates obtained from cross-validation approaches (Stone, 1974), including leave-one-out and k-fold cross-validation. In the context of structural reliability, inputs generally refer to the random variables of the problem, whereas outputs refer to the values obtained by evaluating the LSF, which the metamodel aims to approximate. The mathematical representations of $\hat{G}(\mathbf{x})$ for some common metamodels, namely, RSM, PCE, Kriging, and PC-Kriging, are provided in Table 1.

RSM metamodels refer to a class of metamodels that generate surrogate functions based on simple polynomials, where polynomials up to the second degree, including cross terms as in Eq. (2.24), are commonly used (Khuri & Mukhopadhyay, 2010). Due to their simplicity, they are among the most widely used metamodel approaches (Guimarães, Matos, & Henriques, 2018). The training consists of determining the coefficients of the polynomials, which is generally performed using the least squares method (Hariri-Ardebili, 2018). Since their introduction for structural reliability analysis (Faravelli, 1989), significant improvements to RSM have been proposed (Allaix & Carbone, 2011; Guimarães, Matos, & Henriques, 2018; Roussouly, Petitjean, & Salaun, 2013). RSM metamodels tend to train the models around the equivalent MPFP in original space (Sudret, 2012), implying that the metamodel may only perform well locally around the MPFP. In a quadratic form, without interaction terms (i.e., the rightmost term in Eq. (2.24)), they also suffer from the limitation of only being able to produce one interior maximum, minimum, or saddle point (McDonald et al., 2007). However, RSM metamodels are not limited to the form in Eq. (2.24) and may also be built using other functions, such as spline functions (O'Connell & Wolfinger, 1997) or radial basis functions (Li et al., 2018; McDonald et al., 2007), which can improve the accuracy of the surrogate function globally and for nonlinear functions.

Table 1. Mathematical representations of the surrogate functions for RSM, PCE, Kriging, and PC-Kriging.

Metamodel	Surrogate function representation
RSM	$$\hat{G}(\mathbf{x}) = a + \sum_{i=1}^{n} b_i x_i + \sum_{i=1}^{n} c_i x_i^2 + \sum_{i=1}^{n-1} \sum_{j=i+1}^{n} d_{ij} x_i x_j \quad (2.24)$$ where **x** denotes a vector of n inputs, and a,b_i,c_i, and d_i denote constant coefficients determined via training.
PCE	$$\hat{G}(\mathbf{x}) = \sum_{i=1}^{n} a_i \Psi_i(\mathbf{x}) \quad (2.25)$$ where a_i denotes a series of constant coefficients determined via training, and $\Psi_i(\mathbf{x})$ denotes multivariate orthogonal polynomials.
Kriging	$$\hat{G}(\mathbf{x}) = \sum_{i=1}^{n} a_i f_i(\mathbf{x}) + \sigma^2 Z(\mathbf{x}) \quad (2.26)$$ where $f_i(\mathbf{x})$ are basis or trend functions, $Z(\mathbf{x})$ denotes a zero-mean, unit-variance stationary Gaussian process defined by a set of hyperparameters $\boldsymbol{\theta}$ determined via training, and σ^2 is the Gaussian process variance.
PC-Kriging	$$\hat{G}(x) = \sum_{i=1}^{n} a_i \Psi_i(\mathbf{x}) + \sigma^2 Z(\mathbf{x}) \quad (2.27)$$

PCE metamodels are a class of metamodels that use polynomials orthogonal with respect to the probability distributions of the random variables to represent the surrogate function, and can be viewed as global RSM metamodels (Sudret, 2012). These polynomials are often Hermite polynomials (for normal distributions), Legendre polynomials (for uniform distributions), Laguerre polynomials (for exponential distributions), and Jacobi polynomials (for beta distributions) (Sudret, 2015). These polynomials provide a basis for the PCE representation, which becomes an exact representation of the original function if an infinite series of polynomials is considered (Sudret, 2014). However, in practice, a truncated polynomial series is necessary, which has led to the development of sparse PCE metamodels that aim to produce the optimal sparse basis based on a defined truncation scheme (Blatman & Sudret, 2010, 2011). The use of common polynomial families, such as the Hermite family, is largely founded on an assumption of independence between the random variables of the problem. However, correlations may exist that can cause the convergence of Eq. (2.25) to the original LSF to be significantly impacted, as the polynomials no longer represent an orthogonal basis for the joint probability distribution. This has led to proposals to use orthogonalization approaches, such as the Gram-Schmidt procedure, to construct an orthonormal basis in the original space of the random variables, accounting for dependencies, rather than in standard normal space, as is done when common polynomial families are used (Jakeman et al., 2019). To achieve an accurate global representation of the original LSF, PCE metamodels are commonly trained over the entire input space for the random variables using sampling techniques such as LHS (Chen et al., 2022; Novák, 2022) and QMC sampling (Hariri-Ardebili & Sudret, 2020; Jakeman et al., 2019).

Kriging metamodels, or Gaussian process regression, are interpolation models that assume the LSF follows a Gaussian process, which is a stochastic process where the outputs at any set of inputs follow a joint Gaussian distribution (Teixeira, Nogal, & O'Connor, 2021). Kriging metamodels represent the original function by a trend, the leftmost term in Eq. (2.26), and a stationary Gaussian process with zero mean and unit variance, the rightmost term in Eq. (2.26) (Echard, Gayton, & Lemaire, 2011). Kriging is generally categorized into three types, simple, ordinary, or universal, based on the trend functions (Gaspar, Teixeira, & Guedes Soares, 2017). Simple Kriging refers to the trend being represented by a constant and known value. Ordinary Kriging implies that the trend is constant but its coefficients are unknown and determined via training. Universal Kriging (expressed in Eq. (2.26)) is the most general formulation, in which the trend is represented by a linear combination of known basis functions with coefficients determined through training. Kriging models tend to be trained in the vicinity of the MPFP to obtain an accurate representation of $G(\mathbf{X})=0$ ensuring that the metamodel correctly predicts random variable inputs that yield failure (i.e., providing correct classification) (Guimarães, Matos, & Henriques, 2018). To achieve this, several techniques and so-called learning functions have been developed (Bichon et al., 2008; Echard, Gayton, & Lemaire, 2011; Lv, Lu, & Wang, 2015; Sarmiento et al., 2025; Wang & Wang, 2013) that prioritize inputs from a larger set generated by, for example, LHS or QMC sampling, which are believed to be located near $G(\mathbf{X})=0$. Using such techniques, Kriging metamodels are likely to provide accurate representation of the true function near $G(\mathbf{X})=0$, meaning good local prediction. However, as the distance from training samples in the input space increases, the prediction may become poorer, since it will be more governed by the trend, which, by virtue of the same properties as RSM, can be inefficient at representing nonlinearities.

Recognizing that PCE corresponds to a particular case of universal Kriging, a metamodel referred to as PC-Kriging, in which the PCE becomes the trend function of Kriging, as in Eq. (2.27), has recently been proposed (Schöbi & Sudret, 2014; Schöbi, Sudret, & Wiart, 2015). As such, PC-Kriging combines PCE's ability to represent the global behavior with the local accuracy of Kriging (Schöbi, Sudret, & Marelli, 2017). Since its recent inception, PC-Kriging has received considerable research interest. Further improvements have been suggested, and it has been shown to perform at least as efficiently and accurately as the individual metamodels it combines (Chen et al., 2025; Parisi et al., 2022; Zhang et al., 2023; Zhou & Peng, 2022).

The author's view on the maturity of metamodeling is that the concern is no longer whether metamodels can provide accurate representations of the original function in reliability analysis problems, but rather how efficiently they can do so. This is reflected in the implicit competition that has emerged in studies on the development of new metamodeling approaches, where a model's efficiency is evaluated and compared with other metamodels on examples with known failure probabilities (Guimarães, Matos, & Henriques, 2018; Li et al., 2018; Yun et al., 2020; Zhang et al., 2025; Zhang et al., 2023). Such studies also tend to include more complex examples involving FEA, where accurate metamodels can often be obtained with a few hundred simulations, and sometimes even fewer. They have also been applied in combination with concrete dams (Amini et al., 2021; Hariri-Ardebili & Boodagh, 2019; Hariri-Ardebili & Sudret, 2020; Kang et al., 2022; Khatibinia & Khosravi, 2014; Segura, Padgett, & Paultre, 2020), but to date, their application has been largely limited to studies involving gravity dams.

2.5.4 Sensitivity analysis

Sensitivity analysis not only provides the analyst with an understanding of how changes in input variables influence the output of a model, but also offers intuition into the model itself, which has become increasingly important due to growing model complexity (Saltelli et al., 2020). Sensitivity analysis is also vital with respect to the prioritization of strengthening, modification, and repair techniques (Samarakoon & Ratnayake, 2015). Furthermore, it not only assists in prioritization and disregarding variables, but also serves as an important validation of the model and allows the analyst to identify weaknesses or inconsistencies that may undermine the model's reliability and lead to potential deviations from sound practices (Morales-Torres et al., 2016). To guide these insights, multiple sensitivity measures have been developed, generally categorized as either local or global, with only a selection presented here for brevity, chosen based on their popularity. Local sensitivity measures quantify the effect of small changes in input variables around a specific value or region and are generally most appropriate for models that are approximately linear in that region, since they are typically based on derivatives (Saltelli, Tarantola, & Campolongo, 2000). Global measures explore the full input space by varying parameters across their entire ranges, making them more suitable for complex and nonlinear models than local measures (Saltelli, 2004).

One popular local measure in structural reliability analysis when using FORM is the negative normalized gradient vector $\hat{\boldsymbol{\alpha}}$ as it is a direct byproduct of the analysis. This vector denotes the directional cosines of the MPFP and indicates the contribution of each random variable to the variance of the linearized LSF in the standard normal space (Papaioannou & Straub, 2021). Its components range from -1 to 1, with the magnitude reflecting the variable's importance relative to the others, and the sign reflecting whether the variable contributes to resistance or to demand/load. For independent variables, the negative normalized gradient vector is also valid in the original space, but for correlated variables it must be corrected to account for the transformation from the standard normal space to the original space (Der Kiureghian, 2022).

Another local sensitivity measure is the omission sensitivity factor, γ_i, which is the inverse ratio between the first-order reliability index and the first-order reliability index with a random variable being replaced by a deterministic value x_i^{f} (Madsen, 1988). Defined in Eq. (2.28), it quantifies the approximate change in the reliability index when a random variable is fixed at a deterministic value, while all other variables remain unchanged. The omission sensitivity factor therefore becomes appropriate for variable fixing, where random variables that have little influence on the probability of failure are identified and replaced by deterministic variables (Papaioannou & Straub, 2021).

$$\gamma_i \approx \frac{1+\left(\mathbf{J}_{\mathrm{u,x}}^{\mathrm{T}}\hat{\boldsymbol{\alpha}}\right)_i \left(\mathbf{x}^* - \mathbf{J}_{\mathrm{x,u}}\mathbf{u}^* - \mathbf{x}^{\mathrm{f}}\right)_i \Big/ \beta}{\sqrt{1-\hat{\boldsymbol{\alpha}}^{\mathrm{T}}\mathbf{J}_{\mathrm{u,x}}\left(\mathbf{J}_{\mathrm{x,u}}\mathbf{J}_{\mathrm{x,u}}^{\mathrm{T}}\right)_i \mathbf{J}_{\mathrm{u,x}}^{\mathrm{T}}\hat{\boldsymbol{\alpha}}}} \tag{2.28}$$

where $\mathbf{x}^{\mathrm{f}}$ denotes the vector of deterministic values at which the variables are fixed, and $\mathbf{J}_{\mathrm{u,x}}$ and $\mathbf{J}_{\mathrm{x,u}}$ denote the Jacobians for the transformations from the standard space to the original space and from the original space to the standard space, respectively.

Elasticities of means and standard deviations provide understanding of the influence of the first and second statistical moments of random variable distributions (Lemaire, Chateauneuf, & Mitteau, 2013). Thus, they indicate how the probability of failure is affected by small changes in a random variable's mean or standard deviation, which can help prioritize data collection efforts. These elasticities are obtained as a product of the negative normalized gradient vector and the Jacobian of the probability transformation, as shown in Eq. (2.29)

$$\nabla_{\boldsymbol{\theta}_f}\beta = \hat{\boldsymbol{\alpha}}\,\mathbf{J}_{\mathrm{T},\boldsymbol{\theta}_f}\left(\mathbf{x}^*, \boldsymbol{\theta}_f\right) \tag{2.29}$$

where $\mathbf{J}_{\mathrm{T},\boldsymbol{\theta}_f}\left(\mathbf{x}^*, \boldsymbol{\theta}_f\right)$ is the Jacobian of the probability transformation with respect to the probability distribution parameters $\boldsymbol{\theta}_f$ at the MPFP. Similar to the negative normalized gradient vector, elasticities are local and can take both positive and negative values, indicating whether a change in the mean or standard deviation increases or decreases the probability of failure. Elasticities can also be calculated for deterministic variables in the LSF (Nikolaidis, Ghiocel, & Singhal, 2004).

For global sensitivity analysis, Sobol' indices (Sobol', 1993) are among the most widely used sensitivity measures (Owen, 2014). They are variance-based measures that decompose a model's output variance into contributions from individual input variables, including their interactions, and express these contributions through the variances of conditional expectations (Saltelli et al., 2008). Two types of Sobol' indices are commonly used, the first-order Sobol' index, S_i, and the total-effect Sobol' index, S_i^T, which quantify the contribution of the main effect of a random variable on the model output and the total contribution including its interactions with all other variables, respectively. Eq. (2.30) and Eq. (2.31) provide the general formulations for the first-order and total-effect Sobol' indices, respectively.

$$S_i = \frac{\mathrm{Var}\left[\mathrm{E}\left(Y \mid X_i\right)\right]}{\mathrm{Var}\left(Y\right)} \tag{2.30}$$

$$S_i^T = 1 - \frac{\mathrm{Var}\left[\mathrm{E}\left(Y \mid X_{\sim i}\right)\right]}{\mathrm{Var}\left(Y\right)} \tag{2.31}$$

where Y denotes the output from the function or model, $\mathrm{E}(\cdot)$ denotes the expected value, $\mathrm{Var}(\cdot)$ denotes the variance, and $X_{\sim i}$ represents the set of all input variables except X_i. Interestingly, due to the orthogonality of the PCE basis functions, the Sobol' decompositions can be directly obtained from the calibrated coefficients of the PCE metamodel, making the first-order and total-effect Sobol' indices readily available (Sudret & Mai, 2015). Similarly, in FORM, the squares of the negative normalized gradient vector correspond to both the first-order and the total-effect Sobol' indices since the LSF is a linear approximation (Der Kiureghian, 2022). Other variants of Sobol' indices, which indicate which variable would most improve the accuracy of the probability of failure estimate if known, can be calculated using the reliability index and the negative normalized gradient vector obtained from FORM (Papaioannou & Straub, 2021)

Recognizing that the influence on the output variance of a function or model may not be sufficient to determine the most important variables in some problems, moment-independent measures have been developed (Borgonovo, 2007). Rather than quantifying and ranking variable importance based on statistical moments, moment-independent measures consider the entire output distribution, providing insight into which variable influences the output distribution the most. One such sensitivity measure is the Borgonovo moment-independent importance measure, δ_i, defined in Eq. (2.32), which aims to identify the variable that changes the output distribution the most.

$$\delta_i = \frac{1}{2}\int f_{X_i}\left(x_i\right)\left[\int\left|f_Y\left(y\right) - f_{Y|X_i}\left(y\right)\right|\mathrm{d}y\right]\mathrm{d}x_i \tag{2.32}$$

where $f_{X_i}(x_i)$ is the marginal density of x_i, $f_Y(y)$ is the unconditional density function of the model/function output y, and $f_{Y|X_i}(y)$ is the conditional density of Y given that X_i assumes a fixed value. The integral of Eq. (2.32) is complex and generally has to be solved numerically, which has led to the development of multiple approaches to perform this task (Liu & Homma, 2009; Wei, Lu, & Yuan, 2013; Yun et al., 2019; Yun et al., 2018).

Chapter 3

3. Load capacity and reliability assessment with combined sliding and overturning

To account for the beneficial effects of geometrical irregularities and large-scale asperities in the rock-concrete interface, which are neglected in traditional sliding and overturning analyses discussed in Section 2.2, the use of a failure mode referred to as CSO (combined sliding and overturning) is proposed. The failure mode is first summarized and discussed, along with its analytical formulation, in Section 3.1, which also summarizes a study providing experimental verification of its validity. Its applicability in combination with reliability analysis is discussed in Section 3.2, which also presents an example applying methods from Section 2.5 to assess the reliability of a fictitious dam using both the analytical formulation of the CSO failure mode and FEA.

3.1. Combined sliding and overturning failure mode

3.1.1 Failure behavior for dams with large-scale asperities in the interface

The total shear strength of an interface is the integral of the shear strength over the interface, as expressed in Eq. (2.1). This integral may also be approximated by discretizing the interface into strips, where the sum of the strips' current shear strengths is the total shear strength of the interface. Assuming the Mohr-Coulomb failure criterion, defined in Eq. (2.3), governs the shear capacity of each strip, the inclination θ_R of the resultant reaction force (the sum of the normal and shear forces) relative to the normal of each strip, when the shear strength is fully mobilized, is given in Eq. (3.1).

$$\tan\left(\theta_R\right)=\frac{N_s\mu+cA_s}{N_s}\rightarrow\theta_R=\arctan\left(\mu+\frac{cA_s}{N_s}\right) \tag{3.1}$$

where N_s denotes the normal force acting on the strip and A_s its area. In Eq. (3.1), the numerator is the shear strength of the strip whereas the denominator is the corresponding normal force. For a strip with an inclination, Eq. (3.1) may be rewritten as Eq. (3.2), which gives the inclination $\theta_{R,H}$ of the reaction force, in radians, relative to the horizontal plane.

$$\theta_{R,H} = \frac{\pi}{2} - \alpha - \arctan\left(\mu + \frac{cA_s}{N_s}\right) \tag{3.2}$$

where α denotes the inclination of the interface strip. This inclination $\theta_{R,H}$, shown in Figure 4, corresponds to the direction of the reaction force from the foundation when the shear strength is fully mobilized. For an interface with geometrical irregularities, implying variations in α, the inclination $\theta_{R,H}$ will also differ, indicating a varying reaction force orientation along the interface.

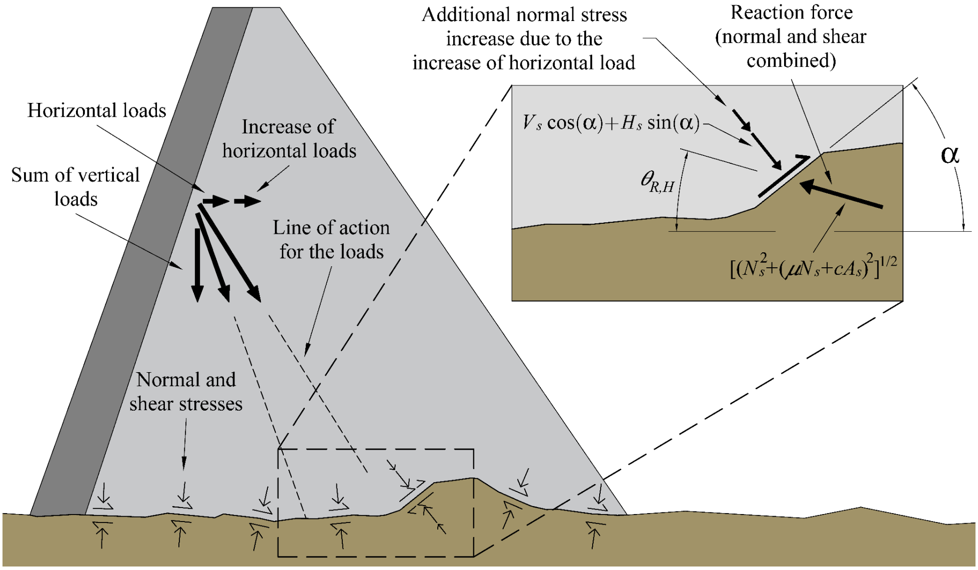

Figure 4. Inclination of the reaction force for an interface with a large-scale asperity.

It is important to note that strips of the interface with more horizontally inclined reaction forces, meaning greater values for α, are better equipped to resist horizontal loads because the normal stress increases with increasing horizontal load. This becomes clear when the normal force is expressed in terms of vertical and horizontal forces that act on the strip, as in Eq. (3.3).

$$N_s = V_s \cos(\alpha) + H_s \sin(\alpha) \rightarrow \tau_f = cA_s + \mu\big(V_s \cos(\alpha) + H_s \sin(\alpha)\big) \tag{3.3}$$

where H_s denotes the horizontal force acting on the strip. Under uniformly distributed vertical loads or rigid body assumptions with the vertical load being greater than the horizontal load per unit area, the shear strength decreases as the inclination α increases.

Under these assumptions, horizontal strips or portions of the interface have greater local shear capacity than inclined portions. Furthermore, the portion with the greatest slope governs global sliding as it would fail first under the assumption of constant shear stresses, as in traditional assessments.

However, for an interface and dam that are stiff but not entirely rigid, small deformations occur once local failure happens, and as the shear capacity increases in proportion to the local inclination for increasing horizontal loads, stresses may redistribute toward more inclined portions of the interface. This reasoning forms the basis of the CSO failure mode, which is formalized and introduced in Paper III. In contrast to traditional sliding analysis, CSO assumes that local failure, deformation, and stress concentration occur along the interface during the development of the failure mode. These assumptions are supported by observations of considerable stress concentrations at large-scale asperities (significant local variations in the interface geometry) in Papers I-II, Paper IV and several studies (Saichi & Bouaanani, 2024; Saichi et al., 2019; Sas et al., 2021; Ulfberg et al., 2022).

In traditional sliding assessments, the effect of a more horizontally aligned reaction force due to the interface's varying inclination can be considered, for example, by expressing the total friction angle of the interface as the sum of the interface's friction angle and α. This approach represents the sliding of the entire dam along a plane with inclination α. However, due to eccentric loading, dams have a natural tendency to rotate and must satisfy moment equilibrium to remain stable, which may result in the approach producing unconservative load capacity estimates.

Combined with the discussion above on local failure and deformation, slight rotations of the dam body, resulting from both global rotation and local deformation, also influence the stress distribution across the interface, as they may cause the dam and foundation to lose, or nearly lose, contact along parts of the interface. At the peak shear capacity of the interface, the inherent assumption of CSO is that stress concentrations in the interface develop at a large-scale asperity, due to its more horizontally inclined reaction force, and at either the heel or the toe of the dam, due to the dam's rotation. This assumption is based on the requirement of at least two points of contact to achieve moment equilibrium. Whether stress concentrations develop at the toe or the heel depends on whether the dam rotates clockwise or counterclockwise, which is determined by the location where the line of action of the loads intersects the interface relative to the asperity

If the line of action intersects the interface downstream of the large-scale asperity, a clockwise rotation (with the upstream side to the left) occurs, and the stress concentrations develop at the toe. The opposite occurs when the line of action intersects the interface in the region between the heel and the large-scale asperity. A third mechanism, involving no rotation, is also assumed possible in CSO. This occurs when the line of action intersects the interface at the upstream face of the large-scale asperity, where the stress concentrations develop. In this case, the dam is assumed not to rotate, as moment equilibrium can be satisfied by the stresses at this section of the interface alone. This case is equivalent to the approach in sliding when the total friction angle of the interface is the sum of the interface's friction angle and α. The evolution of stresses in the interface for increasing horizontal loads, with constant vertical loads, for the CSO failure mode with stress concentrations developing at the toe is depicted in Figure 5(a)-(c). Note that the displacements in Figure 5(c) are exaggerated for illustration purposes.

This behavior was observed in Papers I-II, which analyzed the influence of large-scale asperities in the rock-concrete interface on the load capacity of buttress dams using NLFEA.

In Paper I, NLFEA was employed to study the influence of material parameters on the load capacity obtained from previously reported scale model tests (Sas et al., 2021), in which two of the three buttresses failed by cracking. The three scale models evaluated numerically in Paper I contained either an upstream asperity (referred to as UA in Paper I), a downstream asperity (DA), or both (UDA), with the upstream and downstream asperities having identical shapes across all models. For each model, 64 different combinations of modulus of elasticity, tensile strength, compressive strength, and fracture energy were generated through LHS. Both the DA and UDA models consistently failed due to buttress cracking, and their load capacity was found to be governed by the tensile strength of the buttress concrete. The UA model exhibited a CSO failure behavior, which had not yet been recognized and formalized. Since only parameters related to the buttress concrete were randomized, the material had a negligible influence on the load capacity and affected only the deformation for the UA model.

Significant stress concentrations were observed and reported in Paper I at the downstream asperity with a steep inclination, and an interlocking phenomenon was observed between the buttress and this asperity for the DA and UDA models. This phenomenon can be explained by the fact that both the vertical and horizontal hydrostatic components were increased proportionally until the models failed, effectively preventing the CSO failure mode from fully developing. Consequently, the line of action of the loads changed its inclination only slightly with increased loading, and the evolution shown in Figure 5(a)-(c) did not occur before the buttress ruptured. However, the CSO failure mode had begun to develop, as rotation of the buttresses was observed for the DA and UDA models in Paper I.

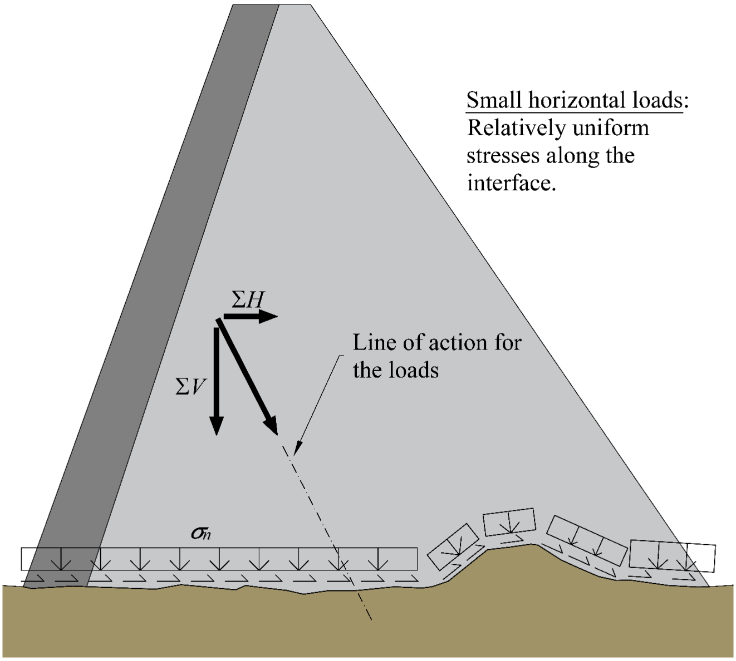
Small horizontal loads:
Relatively uniform stresses along the interface.
ΣH
ΣV
Line of action for the loads
σn

(a)

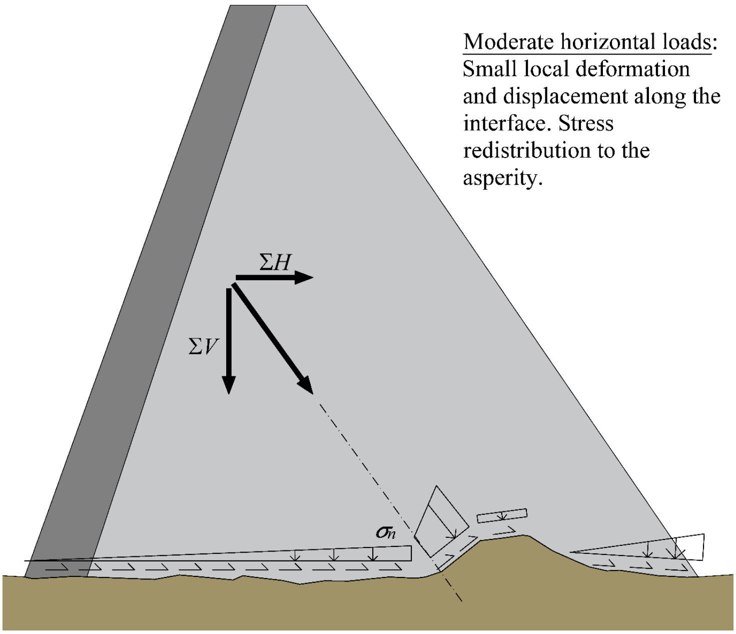
Moderate horizontal loads:
Small local deformation and displacement along the interface. Stress redistribution to the asperity.
ΣH
ΣV
σn

(b)

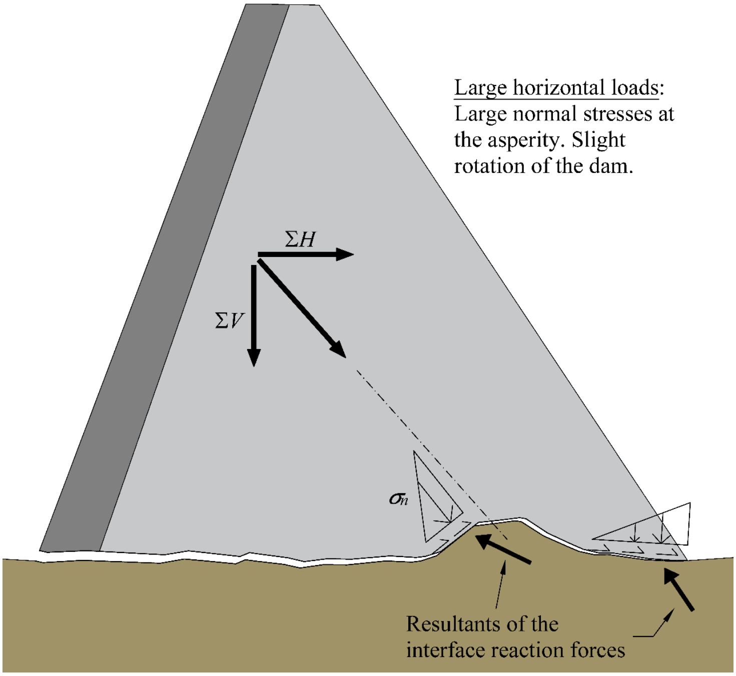

(c)

Figure 5. Evolution of interface stresses for CSO with stress concentrations developing at the toe under: (a) low horizontal loads; (b) moderate horizontal loads; (c) large horizontal loads.

In Paper II, a parametric study was conducted in which the inclination and location of a single large-scale asperity in the interface were varied, along with the model's rock material strengths. After applying the dam's self-weight and hydrostatic pressure, the NLFEA models were brought to failure by increasing the horizontal component of the hydrostatic pressure. Three different types of failure were observed: a global stability failure (referred to as sliding in Paper II), rupture of the concrete in the buttress, or failure of the asperity. The results from Paper II indicate that a greater load capacity is obtained with a greater inclination of the large-scale asperity's upstream face (hereafter referred to as the loaded face) and that asperity locations closer to the toe of the dam were more favorable for inclinations greater than 20 degrees. For lower asperity inclinations, locations closer to the middle of the interface provided greater load capacities.

In the study of Paper II, failure of the asperity became the upper bound for the load capacity and generally occurred for models with steep asperities located closer to the toe in combination with low rock material strength. Rupture of the concrete in the buttress tended to occur for models where the asperity was located closer to the heel of the dam. This failure occurred at load magnitudes greater than the global stability failure but consistently lower than asperity failures. For all three observed failure modes in Paper II, all models exhibited stress concentrations at the large-scale asperity and at the toe or the heel. They also displayed failure behavior involving both rotation and horizontal displacements, and the load capacities of all models were greater than those of a reference model with a completely horizontal interface, which provides results identical to those obtained using the analytical sliding assessment.

Paper III formalized the consistent behavior observed in the models from Papers I-II, where all models exhibited behavior matching that described at the beginning of this section, although some failed preemptively by cracking before the failure mode could fully develop. It also introduces an analytical formulation that allows for large-scale asperities in the rock-concrete interface to be accounted for in the load capacity assessment. In Paper III, the failure is referred to as CSO rather than sliding, to better describe the dam's motions in this failure mode. The analytical formulation relies on the observed stress concentrations at the loaded face of the asperity and at the heel or toe, depending on the rotation of the dam, and assumes that all loads acting on the dam are transferred through the interface in these regions when the failure mode is fully developed. By assuming that all normal stresses in the interface are concentrated at these points, and that the corresponding shear capacity is fully mobilized, the forces acting in these regions of the interface can be calculated using force and moment equilibrium equations.

3.1.2 Analytical assessment of CSO

The process of calculating the load capacity for CSO first involves determining whether a clockwise or counterclockwise rotation occurs. CSO assumes that the loaded face of a large-scale asperity acts as the pivot about which the dam rotates. The direction of rotation can be evaluated either by calculating the sign of the sum of moments about this pivot or by determining where the line of action of the resultant of the forces acting on the dam intersects the interface. In the first approach, the location of the pivot along the loaded face must first be assumed to be either at the base or at the top of the loaded face to satisfy the kinematic constraints imposed by the dam's rotation. Depending on the direction of rotation, the force counteracting the rotation, located either at the toe or the heel, can be calculated using the moment equilibrium model depicted in Figure 6. This force, referred to as the *overturning reaction force* and denoted by F_{O}, represents the resultant of the normal stresses and maintains moment equilibrium for the dam.

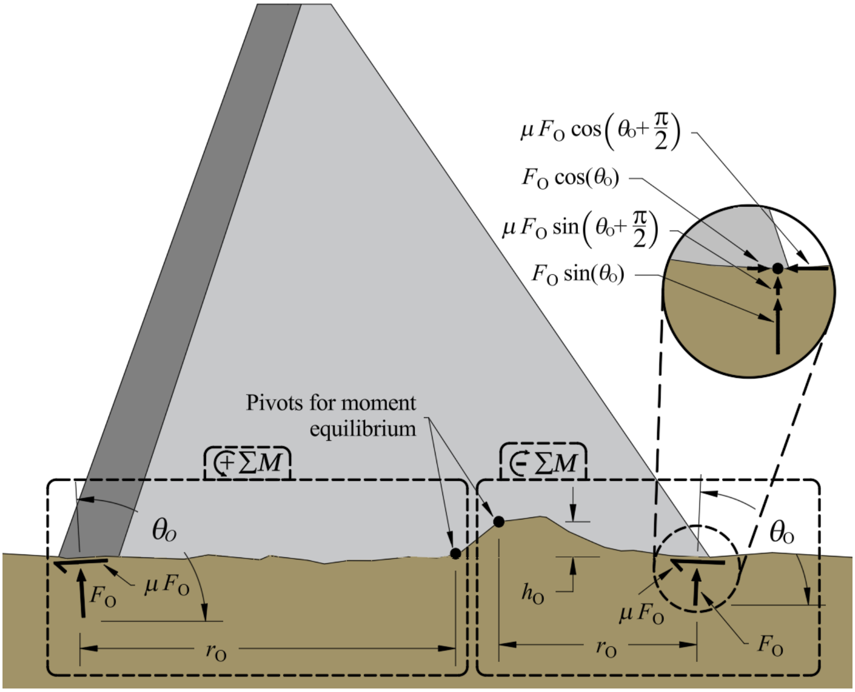

Figure 6. Moment equilibrium model and forces to obtain the overturning reaction force for the CSO failure mode.

In Figure 6, the variables h_O and r_O denote the vertical and horizontal lever arms for F_O, respectively, while θ_O denotes the inclination of the normal to the interface at the location of F_O. Using this model, F_O is determined by Eq. (3.4).

$$F_O = \frac{\left|\sum M\right|}{r_O\left[\sin(\theta_O) + \mu \sin\left(\theta_O + \frac{\pi}{2}\right)\right] \pm h_O\left[\cos(\theta_O) + \mu \cos\left(\theta_O + \frac{\pi}{2}\right)\right]} \tag{3.4}$$

The sign of the rightmost term in the denominator of Eq. (3.4) changes depending on the location of F_O relative to the pivot, as its horizontal component and the corresponding horizontal shear component may either aid or counteract the sum of moments about the pivot. If the line of action intersects the loaded face of the asperity, the sum of the moments becomes relatively small, and the overturning reaction can be assumed to be zero, as the stresses along the loaded face can satisfy moment equilibrium alone. This case represents pure sliding along the loaded face of the asperity. The vertical and horizontal load components, V_O and H_O, respectively, due to F_O may be calculated using Eqs. (3.5) and (3.6).

$$V_O = F_O\left[\sin\left(\theta_O\right) + \mu\sin\left(\theta_O + \frac{\pi}{2}\right)\right] \tag{3.5}$$

$$H_O = F_O\left[\cos\left(\theta_O\right) + \mu\cos\left(\theta_O + \frac{\pi}{2}\right)\right] \tag{3.6}$$

With V_O and H_O determined, evaluating the force equilibrium at the asperity for the forces shown in Figure 7 allows the normal and shear forces at the loaded face of the asperity to be determined.

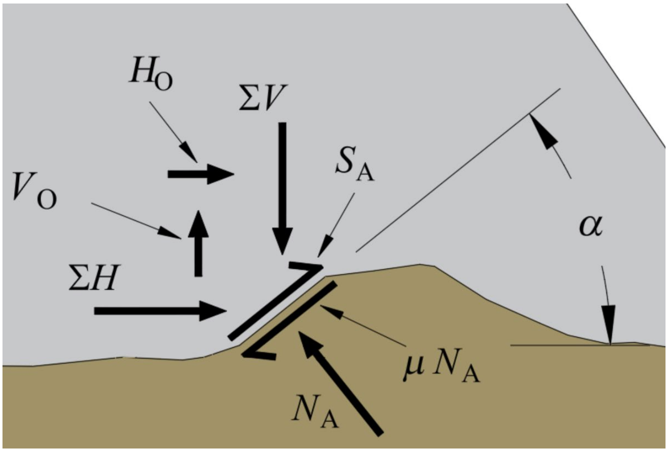

Figure 7. Forces acting on the loaded face of the large-scale asperity.

In Figure 7, α denotes the inclination of the loaded face of the asperity and the normal force N_A and shear force S_A may be determined using Eqs. (3.7) and (3.8), respectively.

$$N_A = \left(\sum V - V_O\right)\cos\left(\alpha\right) + \left(\sum H - H_O\right)\sin\left(\alpha\right) \tag{3.7}$$

$$S_A = \left(\sum H - H_O\right)\cos\left(\alpha\right) - \left(\sum V - V_O\right)\sin\left(\alpha\right) \tag{3.8}$$

Lastly, stability against CSO is evaluated by comparing the shear capacity with the shear force at the loaded face of the asperity using Eq. (3.9), where a positive value indicates stability and a negative value indicates instability.

$$\mu \cdot N_A - S_A \qquad \begin{cases} \text{if } > 0 \rightarrow \text{Stable} \\ \text{if } \leq 0 \rightarrow \text{Unstable} \end{cases} \tag{3.9}$$

Eqs. (3.4)-(3.9) represent the analytical formulation presented for the CSO failure mode in Paper III, in which it is compared against both FEA examples and results from model tests presented in (Ulfberg et al., 2022). The results show that the behavior described at the beginning of this section develops, and that the analytical formulation provides load capacities nearly identical to those obtained from FEA, while also yielding accurate results compared with the scale model tests. The slight discrepancy is believed to be due to differences between the assumed lever arms h_O and r_O in Eq. (3.4) and the corresponding actual lever arms. Since the overturning reaction force is the resultant of the normal stresses at the heel or toe, h_O and r_O should correspond to the distances between the pivot and the resultant. For a completely rigid body, these are the distance from the pivot to the outermost points of the toe and heel, but due to local deformation of the dam and foundation, they are reduced depending on the amount of local deformation. Consequently, an assumption must be made regarding these lever arms, and it should be noted that the maximum capacity for CSO is obtained when they are maximized, implying that they are located at the outermost point on the toe or the heel.

The results of Paper III also show that CSO generally provides load capacities intermediate between those obtained from separate analytical assessments of sliding and overturning, using the methods described in Sections 2.2.1 and 2.2.2. This is illustrated in Figure 8 (adapted from Paper III), which shows the load capacity obtained from FEA (dots), CSO (dashed lines), sliding, and overturning for one of its examples. The figure also illustrates how the location and inclination of the asperity influence the load capacity, where the horizontal axis denotes the asperity's location and α denotes the inclination of its loaded face. The horizontal plateaus in Figure 8 for CSO correspond to cases where the overturning reaction force, obtained from Eq. (3.4), is zero, indicating sliding along the asperity's loaded face. Regions to the left and right of these plateaus correspond to cases where the overturning reaction force is located at the toe or the heel, respectively.

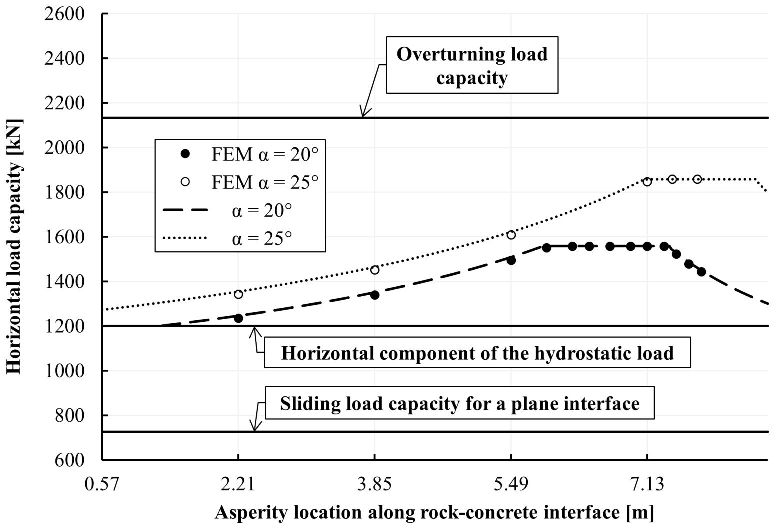

Figure 8. Horizontal load capacity [kN] versus the location of the asperity along the rock-concrete interfaces for asperity inclinations of 20° and 25°. Adapted from Paper III under a Creative Commons CC BY license.

An important observation is that, since CSO uses the same equilibrium equations as sliding and overturning, it may effectively supersede assessments using them individually. Furthermore, under certain conditions, CSO will provide the load capacity of either failure mode. When the inclination α of the loaded face of the large-scale asperity approaches zero, the sliding load capacity is obtained. The overturning load capacity is approached as the large-scale asperity's height decreases, provided it is located at the toe and the interface has sufficiently high shear strength.

An inherent flaw of the load capacity assessment for the CSO failure mode is that it develops through displacements and rotations, while only considering force and moment equilibrium. As a result, other types of failures, such as loss of watertightness due to aperture, may transpire before a CSO failure fully develops. Acknowledging this drawback, Paper III proposes and presents formulations for a magnification factor for the loads based on the direction of the heel's displacement and the use of reduction factors for the lever arms h_O and r_O in Eq. (3.4). The notion behind using magnification factors based on the direction of the heel's displacement relates to the fact that vertical displacements are the main concern with regard to watertightness. The use of reduction factors for the lever arms reflects that the stresses represented by the overturning reaction force converge toward the outermost points of the heel and the toe as the failure mode develops (see Figure 5(a)-(c)). Consequently, instead of the use of arbitrary safety factors to, for example, account for deformations in sliding (USACE, 2005), the load capacity estimate for CSO can be reduced based on the mechanisms inherent to the failure mode.

The analytical formulation for CSO is not limited to simple interfaces with a single large-scale asperity. It can also be applied to cases involving multiple asperities, as shown in Paper III, which also included FEA models with two large-scale asperities. In such cases, the dominant large-scale asperity must be identified and is defined as the asperity that causes the steepest inclination of the heel's displacement, as elaborated on in Paper III. By inducing the steepest displacement, all other large-scale asperities effectively lose contact with the dam, and the load capacity becomes governed by the dominant asperity. As a result, the load capacity for cases with multiple asperities is identical to that for cases where only the dominant asperity is present.

3.1.3 Validation of assumptions for CSO

Building on the formalized CSO failure mode in Paper III, Paper IV presents a study designed to validate the assumptions and hypothesized behavior of CSO beyond the idealized and linear elastic FEA models. The study in Paper IV employed 12 scale models, constructed at a 1:5 scale with an existing Norwegian buttress dam as the prototype, which were subjected to loads equivalent to hydrostatic pressure, ice load, and uplift underneath the front plate. Each model incorporated one of three different rock-concrete interface profiles observed in the prototype dam, selected based on their constructability and the frequency of similarly shaped profiles at the dam's buttresses. These geometries are referred to as G1, G2, and G3, and all included one or more large-scale asperities. Aside from the rock-concrete interface geometries, all scale model geometries were identical.

The scale models in Paper IV were designed using the stress-based scaling approach discussed in Section 2.3, allowing rock bolts and reinforcement to be included and enabling assessment of their influence on the load capacity and behavior of concrete buttress dams. Since the CSO failure mode relies on a large-scale asperity acting as a pivot around which the dam rotates, shallow rock joints beneath the asperities can significantly affect the load capacity and behavior. Therefore, simulated rock joints were also incorporated into some of the scale models, with shapes chosen so that the inclination of the rock joints closest to the downstream side was equal to or lower than that of the loaded face of the asperity. For each interface geometry, the individual scale models were designed with different combinations of rock bolts, reinforcement, and rock joints to assess the influence of each. The scale model nomenclature was based on geometry and an acronym for the included features. For instance, G3-RB-R-RJ denotes a model with G3 geometry that includes rock bolts, reinforcement, and a rock joint in Paper IV.

To assess and validate the assumption of stress concentrations for CSO, the monitoring system included strain gauges and epoxy-coated fiber optic sensors (FOS) which were attached on the dam slightly above the interface profile for each scale model. The strain gauges were placed to measure strains perpendicular to the interface at locations where stress concentrations are assumed to develop for CSO. The FOS was primarily used to measure strains tangential to the interface, but it was also employed to evaluate strains parallel to the front plate near the crest. The placement of the strain gauges and the FOS is shown in Figure 9(a) for scale models with the G1 geometry, along with the corresponding experimental setup, while Figure 9(b) shows a photo of scale model G1-RB-R during the experimental tests.

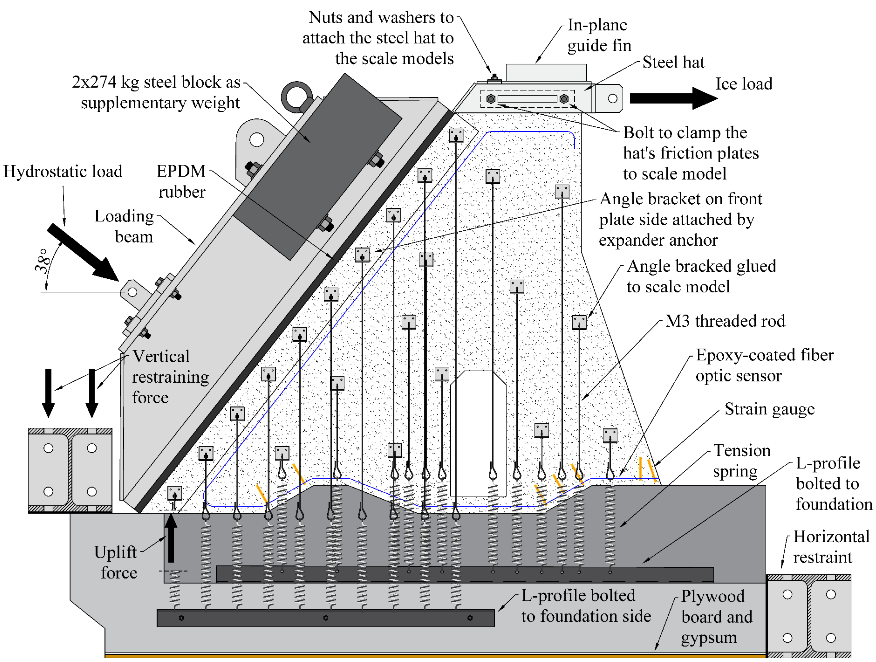

(a)

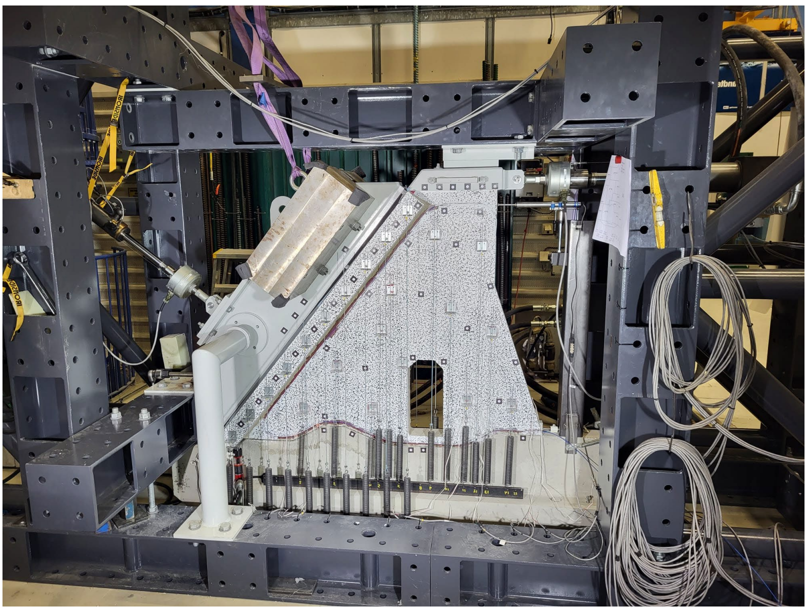

(b)

Figure 9. (a) Experimental set up and location of strain gauges and FOS for scale models with geometry G1 in Paper IV; (b) Photo of experimental test on scale model referred to as G1-RB-R.

To measure horizontal and vertical displacements relative to the foundation for the scale models and assess whether they conform to the hypothesized behavior of CSO, linear variable differential transformers (LVDTs) were placed near the crest, at the heel, toe, and along the interface. These measurements provided insight into the global behavior of the individual scale models. They enabled comparisons of displacements at key points, revealing whether rotation, horizontal movement, or both occurred simultaneously. To supplement the LVDTs, digital image correlation (DIC) was employed, providing a graphical overview of scale model displacements.

The results of the scale model tests presented in Paper IV indicate that the models failed in a manner consistent with the hypothesized CSO failure mode, displaying both rotation and horizontal displacement. This behavior is visible in Figure 10, which shows the displacement vectors obtained from DIC for the scale model referred to as G2-RB shortly after achieving the peak load. The uneven arching pattern indicates that regions near the interface displace less than those near the crest, suggesting rotation. Meanwhile, the similar horizontal lengths of vectors close to the interface indicate a relatively constant horizontal displacement across this region. The LVDTs indicated a similar behavior, recording vertical and horizontal displacements at the heel and horizontal displacements at the crest and toe. The proportions between these displacements varied depending on the scale model geometry, indicating that asperity location and inclination influence the degree of rotation relative to horizontal displacement.

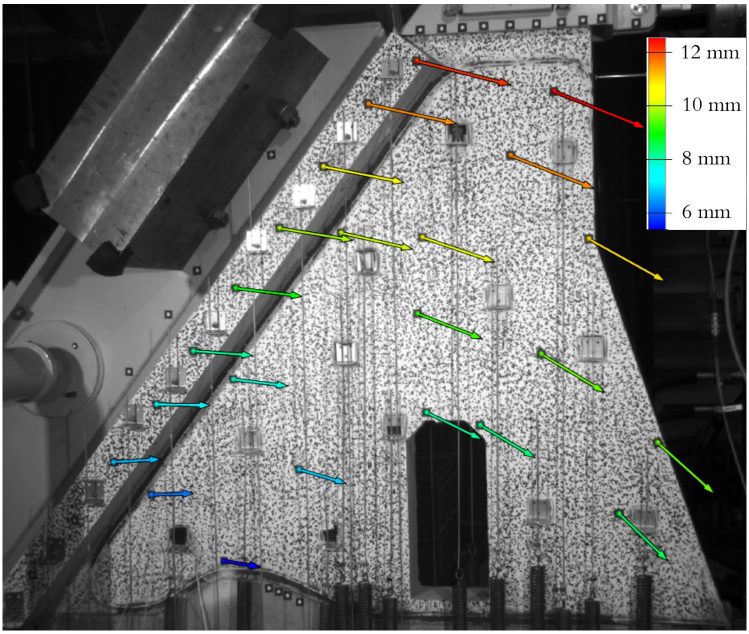

Figure 10. Displacement vectors for scale model G2-RB shortly after reaching the peak load capacity from the study presented in Paper IV.

Strains measured by both the strain gauges and FOS for the scale models, reported in Paper IV, correspond to the assumed stress concentrations for CSO. Notable concentrations were observed at the loaded face of the asperity and at the toe, similar to those depicted in Figure 5(c). These strains also tended to concentrate towards the top of the asperity's loaded face during the progression of the failure, as the strains measured by the strain gauges at the asperity's base decreased and became low or negligible nearing the peak load.

The strain measurements from both the FOS and the strain gauges support the hypothesized phenomenon of a dominant asperity in rock-concrete interfaces with multiple asperities. This is evidenced by negligible strains at the asperity closest to the upstream side at peak load in scale models containing two asperities, indicating that the asperity closest to the downstream side carried most of the load and was the dominant one for those models. Significant tensile strains tangential to the interface, located behind the dominant asperity's loaded face, were captured by the FOS. These strains indicate that the buttress may be at risk of cracking, consistent with the NLFEA models in Papers I-II, in which failures due to the buttress rupturing were observed. However, no cracks were observed near the interface during ocular inspections of the buttress after each scale model test in Paper IV.

The inclusion of reinforcement in the scale models had a negligible influence on the scale models' behavior and load capacity. Cracks that did develop appeared at the crest of the scale models and were regarded as a result of the scale model design, and thus deemed artificial. Rock bolts significantly increased the load capacity of the interface but did not alter the failure behavior and the models still exhibited a CSO type of failure. All three models that included a rock joint had a lower load capacity than their respective counterparts without a rock joint, but only the model referred to as G3-RB-R-RJ in Paper IV experienced a difference in the failure mode. It experienced a failure more consistent with sliding than CSO, as it primarily slid along the rock joint and suggests that rock joints can alter a dam's failure behavior. The scale models with rock joints consisted of three bodies in contact, compared to two in other models, with the rock joint simulated by a concrete prism, referred to as the rock joint prism in Paper IV, that matched the buttress profile and part of the foundation for each geometry. This rock joint prism moved monolithically with the dam body, visible in Figure 11, for all three models with a rock joint. This suggests that CSO may also be applied in such cases by assuming instead that the pivot around which the dam rotates lies along the rock joint rather than at the loaded face of the asperity.

Figure 11. Monolithic behavior and interface gap near the heel and the rock joint prism for scale model G2-RB-R-RJ in Paper IV after having reached its peak load capacity.

Load capacity estimates for sliding, overturning, and CSO for each scale model are presented in Paper IV. As in Paper III, CSO provided results that were more accurate than both sliding and overturning. However, there were some discrepancies between the estimates and the experimentally obtained load capacities. These are believed to be attributed to differences in aspects such as friction angle, strain hardening of the rock bolts, and assumptions regarding the lever arms h_O and r_O in Eq. (3.4).

3.2 Reliability analysis using combined sliding and overturning

3.2.1 Influential parameters for CSO

The studies presented in Papers I–II revealed a consistent behavior of dams with large-scale asperities at the rock-concrete interface, involving a combination of motions assessed in both sliding and overturning. This behavior was then formalized through an analytical formulation in Paper III and experimentally validated in Paper IV. Recognizing the benefits of reliability analysis over deterministic analysis, discussed in Section 2.1, and noting that a better understanding of influential parameters could facilitate a potential implementation of CSO in dam engineering practice, the study presented in Paper V was conducted.

Paper V presents a study on reliability and sensitivity analyses for a simulated population of concrete buttress dam monoliths. The population is based on drawings of Swedish buttress dam monoliths, and the individual samples vary in height, width, front plate inclination, interface inclination, rock bolt area, and other parameters, all randomly generated using QMC sampling. Each sample in the population was assessed deterministically against sliding (Section 2.2.1), overturning (Section 2.2.2), and CSO (using Eqs. (3.4)-(3.9)) for two load cases, either including an ice load or a water level above the crest, representing overtopping. Only resistance variables were included as random variables in the study, due to considerable uncertainties in the statistical distributions of load variables, such as ice load (Hellgren, 2022), and because these variables may depend on factors such as location. The random variables included in the study were the monolith's concrete density, rock bolt yield stress, and two parameters related to the rock-concrete interface friction, namely the basic friction angle and the dilation angle.

Using FORM, the reliability index of each sample was assessed and compared with the corresponding deterministic safety factors in Paper V. For CSO, which was only formalized in Paper III, no deterministic safety measure is defined, and the reliability indices were therefore compared using the ratio between the normal and shear forces, similar to sliding. Local sensitivity measures, such as those described in Section 2.5.4, indicate that the random variables associated with the rock-concrete interface are the most influential with regards to the safety for a dam. This highlights the importance of accurate statistical characterization of these parameters, both for ensuring safety and obtaining reliable estimates of the safety margin. Generally, in Paper V, the least important variable regarding the reliability of the monoliths was the rock bolt yield stress, which only influenced monoliths with a low self-weight, where the rock bolt's contribution to the sum of the resisting loads was greater. Concrete density had a moderate to high influence on monolith reliability, although it was generally less influential than the basic friction angle and dilation angle, which governed the rock-concrete interface friction.

A global sensitivity analysis was also conducted in the study presented in Paper V to assess the influence of the parameters that were varied in the generation of the monolith population, such as their heights and widths, on the monoliths' reliability. To facilitate this, PCE metamodels were used. However, instead of employing them to supplement the LSFs, that assess sliding, overturning, and CSO, they were trained on the reliability indices obtained from the FORM analysis. As such, the PCE metamodels approximated the reliability indices provided by FORM using inputs related to monoliths' shapes, the rock bolt's areas, and deterministic loads for each corresponding LSF. Using the PCE metamodels, the global sensitivity measures described in Section 2.5.4 were estimated, and a one-at-a-time sensitivity analysis was performed to graphically show how the population's median changes with variations in the inputs. The results of the global sensitivity analysis show that the inclination of the front plate generally has a considerable influence on the reliability of buttress dams, with reliability decreasing as the front plate becomes more vertically inclined. For factors influencing only CSO, namely the height, location, and inclination of the large-scale asperity, the inclination of the asperity was the most influential, with steeper inclinations resulting in greater reliability. The location of the asperity also had a considerable influence, with positions between the center of the interface and the toe yielding the greatest reliability. This is due to the phenomenon, elaborated in Paper III, in which load capacity is maximized when the moment about the asperity is minimized, corresponding to sliding along the loaded face of the asperity.

Similar to Papers III–IV, in Paper V, CSO served as an intermediary between sliding and overturning, providing probability of failure estimates between those obtained for sliding and overturning. The probability of failure was generally highest for sliding, whereas overturning generally resulted in negligible probabilities of failure, suggesting that overturning is only relevant in cases where the load magnitude is high, combined with small monolith heights and an almost vertical front plate. Sliding was mainly influenced by the load magnitude, monolith height, thickness of the front plate and buttress, and the inclinations of both the interface and front plate. The lowest reliability was obtained for combinations with high load magnitudes, a less voluminous monolith, a steep upstream inclination, and a downward-sloping interface. By virtue of using similar equilibrium equations, similar combinations related to the height and other parameters apply to CSO. Aspects such as the height of the freeboard, the width of the monoliths, and the area of the rock bolts in the front plate generally had a low influence on reliability for the assessed monolith population.

3.2.2 Application of CSO in reliability-based assessment

The analytical formulation for CSO is straightforward to implement alongside reliability analysis and yields results similar to those of FEA, provided no material failure occurs. Furthermore, the CSO failure mode's LSF, together with the transformation from the original space to the standard normal space for distributions such as the normal and lognormal distributions used in Paper V, is linear or almost linear in standard normal space. Consequently, FORM generally provides sufficiently accurate results when similar distributions are used. This is illustrated by an example in which the reliability of a buttress dam monolith is assessed for its probability of failure when subjected to an ice load of 200 kN/m. Using information presented in Paper V on how the shape of the buttress influences reliability, this example is designed to produce a low reliability for the sliding failure mode. This allows the demonstration of the benefits of considering large-scale asperities in the rock-concrete interface through CSO and highlights the potentially conservative estimates provided by sliding. The geometry of the buttress dam monolith, along with the assumed loads acting on it, is shown in Figure 12.

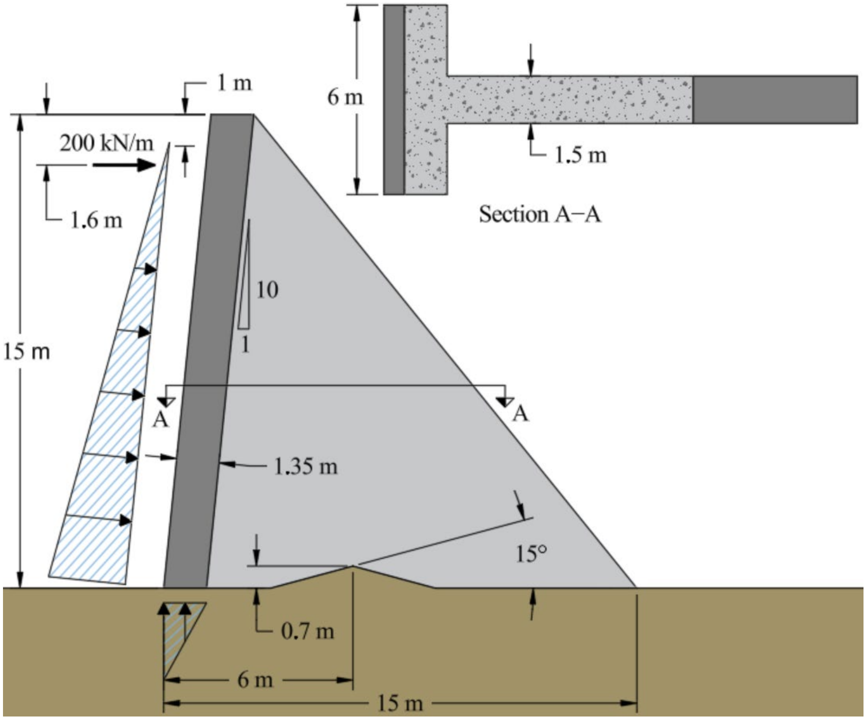

Figure 12. Loads and geometry for the buttress dam monolith in the example.

The reliability of the example monolith in Figure 12 is calculated using different LSFs, namely sliding, CSO, and a PCE metamodel trained on FEA simulations, which are employed in combination with the various methods described in Section 2.5. The overturning failure mode was also assessed, but its probability of failure was too small to be obtained, falling beyond numerical precision, which generally corresponds to β values greater than 8 when using the double-precision format in calculations, as done here. The random variables considered in this example are provided in Table 2 and are based on (Westberg Wilde & Johansson, 2016a). Cohesion is neglected, and the friction of the rock-concrete interface is considered to be the sum of the basic friction angle and the dilation angle, which is here assumed to account for small geometrical irregularities present in the interface.

Table 2. Random variables used in the example comparing FORM, SORM, and FEA in combination with a PCE metamodel with MCS.

Random variable	Symbol	Distribution	Mean	Standard deviation
Basic friction angle [°]	$\phi_{b,c}$	Normal	35	1.75
Dilation angle [°]	i_c	Lognormal	15	3
Concrete density [kN/m^3]	ρ_c	Normal	23.5	0.8

The FEA models were generated using the same procedure outlined in Paper III, with an interface element size of 0.1 m, and no specific boundary conditions were imposed to induce a CSO failure. The deformation and principal minimum stresses, illustrating stress concentrations at the toe, for one of the FEA simulations used to train the PCE metamodel is shown in Figure 13. Note that the displacements are greatly exaggerated for visibility and that the significant principal stress magnitudes at the toe are influenced by the singularity that arises from the sharp geometry of the dam toe.

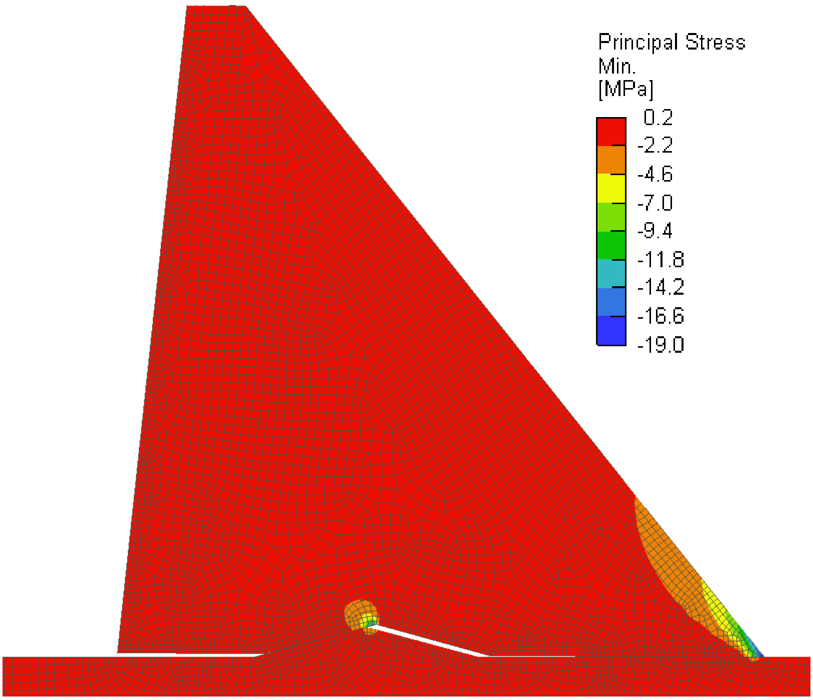

Figure 13. Deformation and principal minimum stresses [MPa] at the peak load for one of the FEA simulations used to train the PCE metamodel.

The results from the reliability analysis of the example are provided in Table 3 for each LSF function along with the reliability method employed. The iHLRF algorithm (Zhang & Der Kiureghian, 1994) was employed in the search for the MPFP in the FORM analysis, and the approximation proposed by Tvedt (Tvedt, 1990), shown in Eq. (2.21), was used to obtain the SORM approximation. The PCE metamodel only needed to be trained on 9 FEA simulations to achieve accurate results, as reflected by a normalized leave-one-out error of less than 10^{-5}. The probability of failure from the calibrated metamodel was calculated using MCS with LHS sampling and 10^7 samples, and the average of 10 MCS runs are provided in Table 3. For the analytical formulation for CSO, the overturning reaction force was assumed to be located at the outermost point of the toe (see Figure 5(c)), meaning that the lever arms h_O and r_O in Eq. (3.4) were 0.7 m and 9 m, respectively.

Table 3. Reliability indices and corresponding probabilities of failure for FORM, SORM, and MCS using a PCE metamodel constructed through FEA simulations.

LSF and reliability method	β	P_f
Sliding with $G = \tan\left(\phi_{\mathrm{b,c}} + i_c\right)\sum V' - \sum H$ FORM using Eq. (2.17)	0.796	0.213
Overturning with $G = \sum M_{\mathrm{S}} - \sum M_{\mathrm{DS}}$	>8	-
CSO with Eqs. (3.4)-(3.9) FORM using Eq. (2.17)	3.483	$2.481 \cdot 10^{-4}$
CSO with Eqs. (3.4)-(3.9) SORM using Eq. (2.21)	3.507	$2.263 \cdot 10^{-4}$
FEA + PCE metamodel using Eq. (2.25) MCS using Eq. (2.23)	3.457	$2.730 \cdot 10^{-4}$

The reliability obtained from analysis of the sliding failure mode indicated that the example buttress monolith in Figure 12 has a 21.3% probability of failure when subjected to an ice load of 200 kN/m, while the probability of failure from overturning is essentially zero. However, when assessing the reliability using the CSO failure mode, the probability of failure becomes 0.025% and 0.023% for FORM and SORM, respectively. These estimates are close to the probability of failure estimate of 0.027% provided by FEA in combination with a PCE metamodel. It is important to note that analytical formulations require an assumed failure behavior, whereas FEA does not, as the behavior is simulated directly. Consequently, incorrect assumptions about the failure mode can lead to inaccurate estimates of load capacity and reliability, as shown in the case of sliding and overturning in Table 3. In contrast, the deformational behavior in the FEA, observed in Figure 13, corresponds to that of the assumed behavior of CSO, shown in Figure 5(c), suggesting an appropriate use of CSO in combination with large-scale asperities. Consequently, a significant gain in reliability over sliding may be obtained. The slight difference between the PCE metamodel and CSO shown in Table 3 is believed to be due to the overturning reaction force being slightly distributed along the toe in the FEA, rather than concentrated at its outermost point as assumed in CSO. Regarding the difference between FORM and SORM, the principal curvatures for the LSF used in the SORM approximation provided in Table 3 were 0.072 and -0.015. A positive curvature indicates that the LSF curves away from the origin, while a negative curvature indicates the opposite. Since the greatest curvature is positive, the linear approximation from FORM yields lower reliability estimates than SORM.

Local sensitivity measures for the example problem using the analytical formulation of CSO are given in Table 4. As indicated by the directional cosines $\hat{\alpha}$ of the negative normalized gradient vector, the most influential random variable for the problem is the dilation angle, closely followed by the basic friction angle. These variables control the majority of the variance, which is also supported by the omission factors γ_i, which correspond to the approximate value for β if the corresponding variable is treated as deterministic and set to its mean value. The elasticities of the means $\nabla\mu_f\beta$ and the standard deviations $\nabla\sigma_f\beta$ for the random variables in Table 4 are scaled by their respective standard deviations. These show that the greatest gain in reliability is obtained when the mean of the dilation angle increases, while the greatest decrease in reliability occurs when its standard deviation increases, further highlighting its importance.

Table 4. Local sensitivity measures obtained from FORM for CSO in the example.

Random variable	$\hat{\alpha}$ Eq. (2.16)	γ_i Eq. (2.28)	$\nabla\mu_f\beta$ Eq. (2.29)	$\nabla\sigma_f\beta$ Eq. (2.29)
ϕ_{rc}	-0.600	4.352	0.602	-1.308
i_c	-0.641	5.150	0.954	-1.557
ρ_c	-0.479	3.968	0.482	-0.835

Global sensitivity measures from the PCE metamodel are provided in Table 5. The first-order Sobol' indices, S_i, and the total-effect Sobol' indices, S_i^T, indicate that there are no interactions between the variables, since they are identical, and that the dilation angle has the highest influence on the variance globally. Similarly, the dilation angle has the greatest influence on the output distribution, meaning the distribution of outcomes for the LSF, as indicated by the Borgonovo moment-independent importance measure δ_i. Thus, the most important variable for the reliability of the example dam monolith is the dilation angle, as it contributes most to the variance and output distribution and has the greatest potential to improve reliability if controlled or known.

Table 5. Global sensitivity measures obtained using the PCE metamodel for the example.

Random variable	S_i Eq. (2.30)	S_i^T Eq. (2.31)	δ_i Eq. (2.32)
ϕ_{rc}	0.178	0.178	0.298
i_c	0.685	0.685	0.417
ρ_c	0.137	0.137	0.283

A general note regarding sensitivity analysis using metamodels is that, if not all relevant coefficients are included in the model, some effects may be missed, and the resulting sensitivity measures may not be entirely accurate (Frey & Patil, 2002). Furthermore, if the metamodel is trained only locally, the sensitivity measures may not be representative of the global behavior, particularly if the true function is nonlinear.

Both the example provided above, and the study presented in Paper V, are time-independent reliability analyses. However, it is acknowledged that dams are subjected to cyclic loads and relatively harsh environments, which in some cases may necessitate a time-dependent reliability analysis to account for potential effects such as material degradation, cumulative damage, and stochastic loading processes. Examples of such effects include seasonal temperature fluctuations, which can induce significant cracking (Nordström et al., 2019), and corrosion of rock bolts, reinforcement, and tendons in ground anchors. These effects can also interact, as widening cracks can increase the corrosion rate (Michel et al., 2016), which in turn may reduce the bond strength between rock bolts or reinforcement and the concrete (Adasooriya, Samarakoon, & Gudmestad, 2017). Such a mechanism is perhaps not relevant to the analytical formulation for CSO, as it only considers equilibrium equations regarding the dam's global stability. However, by using FEA in combination with metamodels, complex time-dependent phenomena can be captured in reliability and sensitivity analyses. Some degradation phenomena can still be applicable to analytical assessment of CSO, such as a potentially decreased shear strength of the rock-concrete interface due to calcium leaching (Buzzi et al., 2008; Lambert, Buzzi, & Giacomini, 2010). For cases where time-dependent reliability analysis is required, the analytical formulation for CSO can be applied directly with either FORM (Gong & Frangopol, 2019) or MCS (Biondini & Frangopol, 2017).

Chapter 4

4. Conclusions

This thesis presents a failure mode for concrete dams that combines the kinematics assessed in sliding and overturning, which are commonly evaluated independently in current practice. The failure mode, referred to as combined sliding and overturning (CSO), is accompanied by an analytical formulation for estimating the load capacity and is relevant for dams with large-scale asperities and geometrical irregularities in the rock-concrete interface. The assumed behavior of the failure mode is formalized, analyzed and verified through both FEA analyses and scale model tests on concrete buttress dams. By explicitly considering large geometrical variations in the rock-concrete interface, the proposed failure mode's analytical formulation provides a more accurate load capacity estimate than those obtained from current analytical assessment practices. Furthermore, by simultaneously considering the equilibrium equations evaluated in sliding and overturning, the combined failure mode may supersede their independent assessment. Since CSO generally provides an intermediate load capacity estimate, its implementation in practice would likely indicate that dams have a greater load capacity than currently perceived. As such, potentially unnecessary strengthening measures may be prevented and the service life of concrete dams prolonged, thereby contributing to sustainability given the significant economic, environmental, and societal value associated with them.

The presented analytical formulation can also be readily implemented in reliability analyses to account for the inherent uncertainties in the field of dam engineering. This is illustrated by the reliability and sensitivity analyses presented, which employ methods such as FORM and SORM to assess the stability of buttress dam monoliths. Consistent with its property of providing an intermediate load capacity estimate, the combined failure mode also yields intermediate reliability compared to sliding and overturning. This reliability estimate is also consistent with the estimates obtained from numerical simulations using FEA and metamodels, provided no material failure occurs, thus offering a simple complement to FEA. The reliability estimate for the combined sliding and overturning failure modes is significantly influenced by parameters related to the friction of the rock-concrete interface, highlighting the need for accurate characterization and representation in assessment. Furthermore, aspects such as the height of the dam, its upstream inclination, and the location and inclination of the large-scale asperities will likely have a significant influence on the reliability of a dam.

Hypothesis:

The hypothesis of the thesis, presented in Section 1.2, was that:

> A concrete buttress dam's load capacity and safety can be more accurately estimated using reliability analysis in combination with FEA or the analytical formulation for CSO, both of which account for the influence of geometrical irregularities and large-scale asperities at interfaces.

The findings from the studies that form the core of this thesis verify this hypothesis. Large-scale asperities in the rock-concrete interface can have a significant influence on the failure behavior, which the sliding and overturning failure modes employed in current practice are not suited to represent. By virtue of misrepresenting the actual failure behavior of concrete dams, they also provide inaccurate load capacity estimates, as shown in the appended papers. However, large-scale asperities can be considered in FEA, as the analysis method is not restricted to presupposed failure behavior and can directly capture their beneficial effect. Furthermore, this effect can also accurately be captured by the analytical formulation for CSO presented in this thesis, providing a simpler complement to FEA.

The existence of an analytical complement is important because it facilitates the use of reliability methods, which often require gradient calculations or repeated evaluations to determine the probability of failure and may not always be feasible or practical when combined with analysis methods such as FEA. CSO is easy to use with reliability analysis, which can explicitly consider the inherent uncertainties in dams. These uncertainties can be considerable, since dams are unique structures with differences in design, geological conditions, and loading. Thus, deterministic approaches that rely on safety factors, which may have been calibrated for dams with different designs and conditions, could provide an inherently inaccurate and unsatisfactory safety. Reliability analysis addresses these issues by evaluating the safety of a dam on a case-by-case basis.

Research questions:

The research questions of the thesis, presented in Section 1.3, were as follows, along with their corresponding answers:

(i) How do geometrical irregularities and large-scale asperities in the rock-concrete interface affect a concrete buttress dam's potential failure behavior?

Geometrical irregularities and large-scale asperities in the rock-concrete interface can lead to a global failure involving both rotation and horizontal displacement, with the asperities controlling the deformation path. This behavior is confirmed by the FEA presented in Papers I-III and by the scale model tests in Paper IV, in which the assessed buttress dam monoliths simultaneously rotated and slid along the interface. The mechanisms behind this behavior and its causes, discussed in Section 3.1 and Paper III, can be summarized as resulting from kinematic constraints and stress redistributions, which may cause significant stress concentrations. These concentrations are likely to occur at the dominant large-scale asperity, defined as the asperity that induces the steepest displacement at the heel for rock-concrete interfaces containing multiple asperities and governs the global failure behavior. Due to these stress concentrations, large-scale asperities may also cause material failures in either the dam or the foundation, as shown by the FEA analyses in Papers I-II, where cracking of the buttress and shearing of the asperity occurred.

(ii) How can geometrical irregularities and large-scale asperities in the rock-concrete interface be accounted for in load capacity assessment of concrete buttress dams?

Nearing a global failure involving both horizontal displacement and rotation, large-scale asperities cause considerable stress concentrations in the rock-concrete interface, indicating that force transfer between the dam and foundation occurs primarily at specific regions. These regions are predictable and can be determined by assessing the sum of moments about the dominant large-scale asperity, which indicates whether a clockwise or counterclockwise rotation will occur. By considering only the stress concentrations and assuming that the shear capacity at these locations is fully mobilized, the peak load capacity can be estimated using simple equilibrium equations. This is the basis for the analytical formulation for CSO, presented in Paper III, which is intended to estimate the load capacity of concrete dams considering large-scale asperities and geometrical irregularities in the rock-concrete interface.

This analytical formulation yields load capacity estimates that are more accurate than those obtained from sliding or overturning assessments and produces results that closely correspond to those of FEA, as illustrated in Paper III and in Section 3.2. However, while the analytical formulation for CSO and FEA both provide similar results for global failures, where the whole monolith or dam section rotates and displaces, the analytical formulation cannot capture material failures as it only considers global force and moment equilibrium. Consequently, in cases where material failure may occur, which becomes more likely for higher asperity inclinations and locations near the front plate, as shown in Papers I-II, NLFEA is more suitable for assessing the load capacity of concrete dams.

(iii) Which parameters related to the resistance and geometry of a buttress dam are most influential for its reliability?

The study presented in Paper V concerns a reliability and sensitivity analysis of a generated population of buttress dam monoliths for two different load cases, using both local and global sensitivity measures described in Section 2.5.4. The study incorporated analytical LSFs with FORM to obtain sensitivity measures related to the random variables, which included the rock-concrete interface's basic friction angle and dilation angle, the density of the concrete, and rock bolt yield stress. By performing the assessment on each sample in a population of buttress dam monoliths, varying aspects such as heights, widths, and front plate inclination, the resulting sensitivity measures formed distributions, and no single input was consistently the most influential. However, the most important random variable among those considered was generally either the dilation angle or the basic friction angle, both influencing the rock-concrete interface's friction. These two variables had the greatest influence on the reliability of the population, while the rock bolt yield stress had a small, and in most cases negligible, effect, due to its generally small contribution to the sum of resisting loads.

In Paper V, PCE metamodels were also trained on the reliability estimates from FORM using the parameters varied in the generation of the monolith population as inputs. This enabled a global sensitivity analysis of the parameters influencing the dam monolith geometry, for which the most important variables were the inclination of the asperity's loaded face and the inclination of the front plate. Parameters that had a moderate influence on the reliability were the location of the asperity, the height of the monolith, and the thickness of the buttress. For material failures, such as rupture of the buttress or the asperities, the tensile strength of the material in question is likely the governing parameter for the load capacity as indicated by the results of Papers I-II.

Chapter 5

5. Future research

The CSO failure mode has been validated for two-dimensional problems, and its corresponding analytical formulation assumes only in-plane movements. However, it may be possible to extend it to three-dimensional problems. In such cases, interaction effects such as those between multiple asperities along the dam or the monolith width are likely to influence the behavior and load capacity and would need to be accounted for in the analytical formulation.

Furthermore, material failure is a likely possibility for dams with large-scale asperities in the interface because of the stress concentrations that develop. This introduces the risk of cracking in either the dam or the foundation, which could cause the dam to fail before the CSO failure mode fully develops. Therefore, suitable approaches with which the analytical formulation can be modified to limit the load capacity and account for material failure are desired. Potential approaches could include calculating the principal stresses at the loaded face of the dominant asperity and imposing limits on their magnitude.

Regarding load capacity reduction factors, CSO develops through rotation and horizontal displacement, and other non-structural failures may occur before the failure mode fully develops. Approaches to limit the load capacity with respect to heel aperture have been proposed with the intent of considering failures such as loss of watertightness, but practical guidelines or rules for determining their size have not been provided. These approaches are related to the failure behavior, either by considering displacement or the evolution of stresses along the interface. As such, some general principles may exist for determining their size.

Furthermore, since stress concentrations arise in predictable areas as the failure mode develops, there may be potential for alarm limits based on strain measurements near the interface.

Concerning statistical descriptions relevant for reliability and sensitivity analysis, there appears to be a lack of knowledge regarding the distributions and statistical moments of parameters, particularly for load actions such as ice load and uplift pressure. Accurate descriptions are, however, essential for obtaining robust estimates in reliability and sensitivity analyses, which warrants further investigation into the statistical characterization of parameters related to dams.

Acknowledgements

The work presented in this thesis was supported and funded by the Swedish Research Council for Sustainable Development (grant 2019-01236) and the Swedish Centre for Sustainable Hydropower (grants VKU32019 and VKU32031) for which the author is grateful. SVC was established by the Swedish Energy Agency, Elforsk and Svenska Kraftnät together with Luleå University, KTH Royal Institute of Technology, Chalmers University of Technology and Uppsala University. http://www.svc.nu.

References

Adasooriya, N., Samarakoon, S., & Gudmestad, O. (2017). Corrosion propagation phase and bond strength degradation of reinforced concrete structures: State of the art. *International Journal of Computational Methods and Experimental Measurements*, *6*, 499-514. https://doi.org/10.2495/CMEM-V6-N3-499-514

Ahmadi, M. T., & Soltani, N. (2021). Mixing Regression-Global Sensitivity analysis of concrete arch dam system safety considering foundation and abutment uncertainties. *Computers and Geotechnics*, *139*, 104368. https://doi.org/10.1016/j.compgeo.2021.104368

Allaix, D. L., & Carbone, V. I. (2011). An improvement of the response surface method. *Structural Safety*, *33*(2), 165-172. https://doi.org/10.1016/j.strusafe.2011.02.001

Allen, D. N. d. G., Chitty, L., Pippard, A. J. S., & Severn, R. T. (1956). The experimental and mathematical analysis of arch dams, with special reference to Dokan. *Proceedings of the Institution of Civil Engineers*, *5*(3), 198-244. https://doi.org/10.1680/iicep.1956.11479

Altarejos-García, L., Escuder-Bueno, I., & Morales-Torres, A. (2015). Advances on the Failure Analysis of the Dam—Foundation Interface of Concrete Dams. *Materials*, *8*(12), 8255-8278. https://www.mdpi.com/1996-1944/8/12/5442

Altarejos-García, L., Escuder-Bueno, I., Serrano-Lombillo, A., & de Membrillera-Ortuño, M. G. (2012). Methodology for estimating the probability of failure by sliding in concrete gravity dams in the context of risk analysis. *Structural Safety*, *36-37*, 1-13. https://doi.org/10.1016/j.strusafe.2012.01.001

Amini, A., Abdollahi, A., Hariri-Ardebili, M. A., & Lall, U. (2021). Copula-based reliability and sensitivity analysis of aging dams: Adaptive Kriging and polynomial chaos Kriging methods. *Applied Soft Computing*, *109*, 107524. https://doi.org/10.1016/j.asoc.2021.107524

Au, S.-K., & Beck, J. L. (2001). Estimation of small failure probabilities in high dimensions by subset simulation. *Probabilistic Engineering Mechanics*, *16*(4), 263-277. https://doi.org/10.1016/S0266-8920(01)00019-4

Barpi, F., & Valente, S. (2000). Numerical Simulation of Prenotched Gravity Dam Models. *Journal of Engineering Mechanics*, *126*(6), 611-619.

Barpi, F., Valente, S., Ferrara, G., & Imperato, L. (1998). *Experimental and numerical evaluation of gravity dam model failure lifetime* FraMCoS 3, Japan.

Bažant, Z. P. (1984). Size Effect in Blunt Fracture: Concrete, Rock, Metal. *Journal of Engineering Mechanics*, *110*(4), 518-535. https://doi.org/10.1061/(ASCE)0733-9399(1984)110:4(518)

Bichon, B. J., Eldred, M. S., Swiler, L. P., Mahadevan, S., & McFarland, J. M. (2008). Efficient Global Reliability Analysis for Nonlinear Implicit Performance Functions. *AIAA Journal*, *46*(10), 2459-2468. https://doi.org/10.2514/1.34321

Biondini, F., & Frangopol, D. M. (2017). Time-variant redundancy and failure times of deteriorating concrete structures considering multiple limit states. *Structure and Infrastructure Engineering*, *13*(1), 94-106. https://doi.org/10.1080/15732479.2016.1198403

Bjerager, P. (1988). Probability Integration by Directional Simulation. *Journal of Engineering Mechanics*, *114*(8), 1285 - 1302. https://doi.org/10.1061/(ASCE)0733-9399(1988)114:8(1285)

Bjerager, P. (1990). On computation methods for structural reliability analysis. *Structural Safety*, *9*(2), 79-96. https://doi.org/10.1016/0167-4730(90)90001-6

Blatman, G., & Sudret, B. (2010). An adaptive algorithm to build up sparse polynomial chaos expansions for stochastic finite element analysis. *Probabilistic Engineering Mechanics*, *25*(2), 183-197. https://doi.org/10.1016/j.probengmech.2009.10.003

Blatman, G., & Sudret, B. (2011). Adaptive sparse polynomial chaos expansion based on least angle regression. *Journal of Computational Physics*, *230*(6), 2345-2367. https://doi.org/10.1016/j.jcp.2010.12.021

Borgonovo, E. (2007). A new uncertainty importance measure. *Reliability Engineering & System Safety*, *92*(6), 771-784. https://doi.org/10.1016/j.ress.2006.04.015

Breitung, K. (1984). Asymptotic Approximations for Multinormal Integrals. *Journal of Engineering Mechanics*, *110*(3), 357-366. https://doi.org/10.1061/(ASCE)0733-9399(1984)110:3(357)

Buzzi, O., Boulon, M., Hervé, M., & Su, K. (2008). Leaching of rock-concrete interfaces. *Rock Mechanics and Rock Engineering*, *41*(3), 445-466. https://doi.org/10.1007/s00603-007-0156-5

CDA. (2013). *Dam Safety Guidelines 2007*.

CEN. (2006). *Basis of Structural Design, Eurocode 0* (EN 1990, Issue.

CFGB. (2002). *Small dams - Guidelines for Design, Construction and Monitoring*.

Chen, J., Chen, Z., Jiang, W., Guo, H., & Chen, L. (2025). A reliability-based design optimization strategy using quantile surrogates by improved PC-kriging. *Reliability Engineering & System Safety*, *253*, 110491. https://doi.org/10.1016/j.ress.2024.110491

Chen, M., Zhang, X., Shen, K., & Pan, G. (2022). Uncertainty quantification and global sensitivity analysis for composite cylinder shell via data-driven polynomial chaos expansion. *Journal of Physics: Conference Series*, *2174*(1), 012085. https://doi.org/10.1088/1742-6596/2174/1/012085

Chen, Y., Zhang, L., Yang, B., Dong, J., & Chen, J. (2015). Geomechanical model test on dam stability and application to Jinping High arch dam. *International Journal of Rock Mechanics and Mining Sciences*, *76*, 1-9. https://doi.org/10.1016/j.ijrmms.2015.01.001

Chen, Y., Zhang, L., Yang, G., Dong, J., & Chen, J. (2012). Anti-sliding stability of a gravity dam on complicated foundation with multiple structural planes. *International Journal of Rock Mechanics and Mining Sciences*, *55*, 151-156. https://doi.org/10.1016/j.ijrmms.2012.07.010

Chen, Z., Huang, D., Li, X., Qiu, G., & Zhao, P. (2024). A reliability analysis method based on the intersection area division of hypersphere and paraboloid. *Reliability Engineering & System Safety*, *252*, 110461. https://doi.org/10.1016/j.ress.2024.110461

Choi, C. K., & Kwak, H. G. (1990). The effect of finite element mesh size in nonlinear analysis of reinforced concrete structures. *Computers & Structures*, *36*(5), 807-815. https://doi.org/10.1016/0045-7949(90)90151-Q

Choi, S.-K., Grandhi, R., & Canfield, R. (2007). *Reliability-based Structural Design*. Springer London. https://doi.org/10.1007/978-1-84628-445-8_4

De Sortis, A., & Paoliani, P. (2007). Statistical analysis and structural identification in concrete dam monitoring. *Engineering Structures*, *29*(1), 110-120. https://doi.org/10.1016/j.engstruct.2006.04.022

Der Kiureghian, A. (2022). *Structural and System Reliability*. Cambridge University Press.

Der Kiureghian, A., & De Stefano, M. (1991). Efficient Algorithm for Second-Order Reliability Analysis. *Journal of Engineering Mechanics*, *117*(12), 2904-2923. https://doi.org/10.1061/(ASCE)0733-9399(1991)117:12(2904)

Echard, B., Gayton, N., & Lemaire, M. (2011). AK-MCS: An active learning reliability method combining Kriging and Monte Carlo Simulation. *Structural Safety*, *33*(2), 145-154. https://doi.org/10.1016/j.strusafe.2011.01.002

Ellingwood, B., Maes, M., Michael Bartlett, F., Beck, A. T., Caprani, C., Der Kiureghian, A., Dueñas-Osorio, L., Galvão, N., Gilbert, R., Li, J., Matos, J., Mori, Y., Papaioannou, I., Parades, R., Straub, D., & Sudret, B. (2025). Development of methods of structural reliability. *Structural Safety*, *113*, 102474. https://doi.org/10.1016/j.strusafe.2024.102474

Enzell, J. (2023). *Toward Realistic Failure Evaluations for Concrete Buttress Dams* [Licentiate Thesis, KTH Royal Institute of Technology]. Stockholm, Sweden.

Enzell, J., Ulfberg, A., Sas, G., & Malm, R. (2021). Post-peak behavior of concrete dams based on nonlinear finite element analyses. *Engineering Failure Analysis*, *130*, 105778. https://doi.org/10.1016/j.engfailanal.2021.105778

Faravelli, L. (1989). Response Surface Approach for Reliability Analysis. *Journal of Engineering Mechanics*, *115*(12), 2763-2781. https://doi.org/10.1061/(ASCE)0733-9399(1989)115:12(2763)

Faure, H. (1981). Discrépances de suites associées à un système de numération (en dimension un). *Bulletin de la Société Mathématique de France*, *109*, 143-182. https://doi.org/10.24033/bsmf.1935

Fei, W.-P., Zhang, L., & Zhang, R. (2010). Experimental study on a geo-mechanical model of a high arch dam. *International Journal of Rock Mechanics and Mining Sciences*, *47*(2), 299-306. https://doi.org/10.1016/j.ijrmms.2009.12.005

FERC. (2016). *Engineering Guidelines for the Evaluation of Hydropower Projects*.

Ferreira, G. F., Freitas, M. S., Rocha, J. A., & Sisquini, G. R. (2019). SORM DG—An efficient SORM based on differential geometry. *REM International Engineering Journal*, *72*(4). https://doi.org/10.1590/0370-44672018720171

Fishman, Y. A. (1979). Investigations Into The Mechanism Of The Failure Of Concrete Dams Rock Foundations And Their Stability Analysis. 4th ISRM Congress,

Fishman, Y. A. (1988). New Method of Stability Analysis of Concrete Dams on Rock Foundations. ISRM International Symposium,

Fishman, Y. A. (2008). Features of shear failure of brittle materials and concrete structures on rock foundations. *International Journal of Rock Mechanics and Mining Sciences*, *45*(6), 976-992. https://doi.org/10.1016/j.ijrmms.2007.09.011

Frey, C. H., & Patil, S. R. (2002). Identification and Review of Sensitivity Analysis Methods. *Risk Analysis*, *22*(3), 553-578. https://doi.org/10.1111/0272-4332.00039

Fu, C., & Hafliðason, B. (2015). *Progressive failure analyses of concrete buttress dams : Influence of crack propagation on the structural dam safety* [Master Thesis, KTH Royal Institute of Technology]. Stockholm, Sweden.

Fumagalli, E. (1966). Stability of Arch Dam Rock Abutments. 1st ISRM Congress,

Fumagalli, E. (1973). *Statical and Geomechanical Models*. Springer-Verlag Wien. https://doi.org/10.1007/978-3-7091-8317-5

Gao, Z., Wang, G., Lu, W., Liu, S., Pan, X., & Qi, Z. (2025). A new impact factor considering structural morphology for concrete gravity dams subjected to underwater non-contact explosion. *Engineering Structures*, *341*, 120826. https://doi.org/10.1016/j.engstruct.2025.120826

Gaspar, B., Teixeira, A. P., & Guedes Soares, C. (2017). Adaptive surrogate model with active refinement combining Kriging and a trust region method. *Reliability Engineering & System Safety*, *165*, 277-291. https://doi.org/10.1016/j.ress.2017.03.035

Gong, C., & Frangopol, D. M. (2019). An efficient time-dependent reliability method. *Structural Safety*, *81*, 101864. https://doi.org/10.1016/j.strusafe.2019.05.001

Guimarães, H., Matos, J. C., & Henriques, A. A. (2018). An innovative adaptive sparse response surface method for structural reliability analysis. *Structural Safety*, *73*, 12-28. https://doi.org/10.1016/j.strusafe.2018.02.001

Halton, J. H. (1960). On the efficiency of certain quasi-random sequences of points in evaluating multi-dimensional integrals. *Numerische Mathematik*, *2*(1), 84-90. https://doi.org/10.1007/BF01386213

Harbitz, A. (1986). An efficient sampling method for probability of failure calculation. *Structural Safety*, *3*(2), 109-115. https://doi.org/10.1016/0167-4730(86)90012-3

Hariri-Ardebili, M. A. (2018). Risk, Reliability, Resilience (R3) and beyond in dam engineering: A state-of-the-art review. *International Journal of Disaster Risk Reduction*, *31*, 806-831. https://doi.org/10.1016/j.ijdrr.2018.07.024

Hariri-Ardebili, M. A., & Boodagh, P. (2019). Taguchi design-based seismic reliability analysis of geostructures. *Georisk: Assessment and Management of Risk for Engineered Systems and Geohazards*, *13*(1), 34-52. https://doi.org/10.1080/17499518.2018.1478106

Hariri-Ardebili, M. A., & Sudret, B. (2020). Polynomial chaos expansion for uncertainty quantification of dam engineering problems. *Engineering Structures*, *203*, 109631. https://doi.org/10.1016/j.engstruct.2019.109631

Harris, D. W., & Travers, F. (2006). *Investigation of the Failure Modes of Concrete Dams - Physical Model Tests*.

Harris, H. G., & Sabnis, G. M. (1999). *Structural Modelling and Experimental Techniques* (2 ed.). CRC Press.

Hellgren, R. (2022). *A systems approach to ice loads on concrete dams* [Doctoral Thesis, KTH Royal Institute of Technology]. Stockholm, Sweden.

Hohenbichler, M., & Rackwitz, R. (1988). Improvement Of Second-Order Reliability Estimates by Importance Sampling. *Journal of Engineering Mechanics*, *114*(12), 2195-2199. https://doi.org/10.1061/(ASCE)0733-9399(1988)114:12(2195)

Huang, C. W., El Hami, A., & Radi, B. (2017a). Overview of Structural Reliability Analysis Methods — Part I : Local Reliability Methods. *Incertitudes et fiabilité des systèmes multiphysiques*, *17*. https://doi.org/10.21494/ISTE.OP.2017.0115

Huang, C. W., El Hami, A., & Radi, B. (2017b). Overview of Structural Reliability Analysis Methods — Part II : Sampling Methods. *Incertitudes et fiabilité des systèmes multiphysiques*, *17*. https://doi.org/10.21494/ISTE.OP.2017.0116

Huang, C. W., El Hami, A., & Radi, B. (2017c). Overview of Structural Reliability Analysis Methods — Part III : Global Reliability Methods. *Incertitudes et fiabilité des systèmes multiphysiques*, *17*. https://doi.org/10.21494/ISTE.OP.2017.0117

Huang, X. (2024). Damage effect of underwater explosion bubble on concrete gravity dam. *Engineering Failure Analysis*, *163*, 108516. https://doi.org/10.1016/j.engfailanal.2024.108516

Hurtado, J. (2013). *Structural Reliability*. Springer-Verlag, Heidelberg.

Hussein, T. S., Al-Husseini, T. R., Mousa, M. A., & Al-Jelawy, H. M. (2025). Comparative analysis of stochastic variables for seismic vulnerability assessment of concrete gravity dams. *Multiscale and Multidisciplinary Modeling, Experiments and Design*, *8*(5), 242. https://doi.org/10.1007/s41939-025-00840-0

ICOLD. (2013). *Bulletin 155: Guidelines for use of Numerical Models in Dam Engineering*.

IEA. (2021). *Hydropower Special Market Report - Analysis and forecast to 2030*.

Iman, R. L., & Hora, S. C. (1990). A Robust Measure of Uncertainty Importance for Use in Fault Tree System Analysis. *Risk Analysis*, *10*(3), 401-406. https://doi.org/10.1111/j.1539-6924.1990.tb00523.x

IS. (2019). *Criteria for Design of Solid Gravity Dams*. B. o. I. Standards.

Jakeman, J. D., Franzelin, F., Narayan, A., Eldred, M., & Plfüger, D. (2019). Polynomial chaos expansions for dependent random variables. *Computer Methods in Applied Mechanics and Engineering*, *351*, 643-666. https://doi.org/10.1016/j.cma.2019.03.049

Jiang, H., Lu, W., Wang, G., Wu, L., & Liu, J. (2025). Damage mechanism of model arch dam subjected to far-field underwater explosion. *Engineering Structures*, *322*, 119081. https://doi.org/10.1016/j.engstruct.2024.119081

Johansson, F. (2009). *Shear Strength of Unfilled and Rough Rock Joints in Sliding Stability Analyses of Concrete Dams* [Doctoral Thesis, KTH Royal Institute of Technology]. Stockholm, Sweden.

Kang, F., Liu, X., Li, J., & Li, H. (2022). Multi-parameter inverse analysis of concrete dams using kernel extreme learning machines-based response surface model. *Engineering Structures*, *256*, 113999. https://doi.org/10.1016/j.engstruct.2022.113999

Khaneghahi, M. H., Alembagheri, M., & Soltani, N. (2019). Reliability and variance-based sensitivity analysis of arch dams during construction and reservoir impoundment. *Frontiers of Structural and Civil Engineering*, *13*(3), 526-541. https://doi.org/10.1007/s11709-018-0495-1

Khatibinia, M., & Khosravi, S. (2014). A hybrid approach based on an improved gravitational search algorithm and orthogonal crossover for optimal shape design of concrete gravity dams. *Applied Soft Computing*, *16*, 223-233. https://doi.org/10.1016/j.asoc.2013.12.008

Khuri, A. I., & Mukhopadhyay, S. (2010). Response surface methodology. *WIREs Computational Statistics*, *2*(2), 128-149. https://doi.org/10.1002/wics.73

Koutsourelakis, P. S., Pradlwarter, H. J., & Schuëller, G. I. (2004). Reliability of structures in high dimensions, part I: algorithms and applications. *Probabilistic Engineering Mechanics*, *19*(4), 409-417. https://doi.org/10.1016/j.probengmech.2004.05.001

Krounis, A. (2016). *Sliding stability re-assessment of concrete dams with bonded concrete-rock interfaces* [Doctoral Thesis, KTH Royal Institute of Technology]. Stockholm, Sweden.

Lambert, C., Buzzi, O., & Giacomini, A. (2010). Influence of calcium leaching on the mechanical behavior of a rock–mortar interface: A DEM analysis. *Computers and Geotechnics*, *37*(3), 258-266. https://doi.org/10.1016/j.compgeo.2009.09.006

Lemaire, M., Chateauneuf, A., & Mitteau, J. C. (2013). *Structural Reliability*. Wiley.

Lemos, J. V., Pina, C. A. B., Costa, C. P., & Gomes, J. P. (1995). An Experimental Study of an Arch Dam On a Jointed Foundation. 8th ISRM Congress.

Li, X., Gong, C., Gu, L., Gao, W., Jing, Z., & Su, H. (2018). A sequential surrogate method for reliability analysis based on radial basis function. *Structural Safety*, *73*, 42-53. https://doi.org/10.1016/j.strusafe.2018.02.005

Li, Z. (2021). Global Sensitivity Analysis of the Static Performance of Concrete Gravity Dam from the Viewpoint of Structural Health Monitoring. *Archives of Computational Methods in Engineering*, *28*(3), 1611-1646. https://doi.org/10.1007/s11831-020-09434-0

Li, Z., Lei, D., & Huang, Z. (2024). Effect of boundary conditions on the centrifugal model of concrete gravity dams subjected to underwater explosion. *Engineering Failure Analysis*, *157*, 107902. https://doi.org/10.1016/j.engfailanal.2023.107902

Liu, A., Wang, G., Lu, W., Qi, Z., Zhu, S., Mao, Y., & Gao, Z. (2025). Experimental investigation on protection measures of concrete gravity dams subjected to underwater explosion. *Engineering Structures*, *345*, 121478. https://doi.org/10.1016/j.engstruct.2025.121478

Liu, J., Feng, X.-T., Ding, X.-L., Zhang, J., & Yue, D.-M. (2003). Stability assessment of the Three-Gorges Dam foundation, China, using physical and numerical modeling—Part I: physical model tests. *International Journal of Rock Mechanics and Mining Sciences*, *40*(5), 609-631. https://doi.org/10.1016/S1365-1609(03)00055-8

Liu, Q., & Homma, T. (2009). A new computational method of a moment-independent uncertainty importance measure. *Reliability Engineering & System Safety*, *94*(7), 1205-1211. https://doi.org/10.1016/j.ress.2008.10.005

Liu, Y., Zhang, H., Zheng, D., Cao, E., & Kuai, P. (2020). Sensitivity analysis and instability study of mechanical parameters of deterioration layer of RCC dam. *IOP Conference Series: Earth and Environmental Science*, *560*(1), 012075. https://doi.org/10.1088/1755-1315/560/1/012075

Liu, Y. R., Guan, F. H., Yang, Q., Yang, R. Q., & Zhou, W. Y. (2013). Geomechanical model test for stability analysis of high arch dam based on small blocks masonry technique. *International Journal of Rock Mechanics and Mining Sciences*, *61*, 231-243. https://doi.org/10.1016/j.ijrmms.2013.03.003

Lv, Z., Lu, Z., & Wang, P. (2015). A new learning function for Kriging and its applications to solve reliability problems in engineering. *Computers & Mathematics with Applications*, *70*(5), 1182-1197. https://doi.org/10.1016/j.camwa.2015.07.004

Madsen, H. O. (1988). Omission sensitivity factors. *Structural Safety*, *5*(1), 35-45. https://doi.org/10.1016/0167-4730(88)90004-5

Malm, R. (2016). *Guideline for FE analyses of concrete dams*.

Mansour, R. (2016). *Reliability Assessment and Probabilistic Optimization in Structural Design* [Doctoral Thesis, KTH Royal Institute of Technology]. Stockholm, Sweden.

Mansour, R., & Olsson, M. (2014). A Closed-Form Second-Order Reliability Method Using Noncentral Chi-Squared Distributions. *Journal of Mechanical Design*, *136*(10). https://doi.org/10.1115/1.4027982

McDonald, D., B. , Grantham, W., J., Tabor, W., L., & Murphy, M., J. (2007). Global and local optimization using radial basis function response surface models. *Applied Mathematical Modelling*, *31*(10), 2095-2110. https://doi.org/10.1016/j.apm.2006.08.008

McKay, M. D., Beckman, R. J., & Conover, W. J. (1979). Comparison of Three Methods for Selecting Values of Input Variables in the Analysis of Output from a Computer Code. *Technometrics*, *21*(2), 239-245. https://doi.org/10.1080/00401706.1979.10489755

Melchers, R. E., & Beck, A. T. (2018). *Structural reliability analysis and prediction* (third ed ed.). John wiley & sons.

Mencik, J. (2016). *Concise Reliability for Engineers*. IntechOpen. https://doi.org/10.5772/62009

Michel, A., Otieno, M., Stang, H., & Geiker, M. R. (2016). Propagation of steel corrosion in concrete: Experimental and numerical investigations. *Cement and Concrete Composites*, *70*, 171-182. https://doi.org/10.1016/j.cemconcomp.2016.04.007

Modéer, M. (1979). *A fracture mechanics approach to failure analyses of concrete materials* (Publication Number TVBM-1001) [Doctoral Thesis, Lund University]. Lund, Sweden.

Morales-Torres, A., Escuder-Bueno, I., Altarejos-García, L., & Serrano-Lombillo, A. (2016). Building fragility curves of sliding failure of concrete gravity dams integrating natural and epistemic uncertainties. *Engineering Structures*, *125*, 227-235. https://doi.org/10.1016/j.engstruct.2016.07.006

Muda, Z. C., Hafez, M., Sidek, L. M., Basri, H., Beddu, S., Omar, S. M. A., Almkahar, Z., & Zakaria, A. a. (2024). A Reliability-Based Risk Analysis of a Hollow Buttress Gravity Concrete Dam. *Applied Mathematics and Information Science*, *18*(5), 1161-1178.

Nataf, A. (1962). Détermination des distributions dont les marges sont données. *Comptes Rendus Académie des Sciences*(225).

Nelsen, R. B. (2006). *An Introduction to Copulas* (second ed. ed.). Springer.

Nicholson, G. (1983). *Design of gravity dams on rock foundations: Sliding stability assessment by limit equilibrium and selection of shear strength parameters*.

Nikolaidis, E., Ghiocel, D. M., & Singhal, S. N. (2004). *Engineering Design Reliability Handbook*. CRC Press.

Nordström, E., Hassanzadeh, M., Malm, R., Ekström, T., & Janz, M. (2019). *Structural Safety of Cracked Concrete Dams*. https://doi.org/10.13140/RG.2.2.29067.44329

Novák, L. (2022). On distribution-based global sensitivity analysis by polynomial chaos expansion. *Computers & Structures*, *267*, 106808. https://doi.org/10.1016/j.compstruc.2022.106808

Nowak, A., & Collins, K. (2013). *Reliability of Structures*. Taylor & Francis Ltd. https://doi.org/10.1201/b12913

NVE. (2005). *Retningslinjer for betongdammer til § 4.8 i forskrift om sikkerhet og tilsyn med vassdragsanlegg*.

O'Connell, M. A., & Wolfinger, R. D. (1997). Spatial Regression Models, Response Surfaces, and Process Optimization. *Journal of Computational and Graphical Statistics*, *6*(2), 224-241. https://doi.org/10.2307/1390932

Oberti, G., & Fumagalli, E. (1979). Static Geomechanical Model Of The Ridracoli Arch Gravity Dam. 4th ISRM Congress,

Oliveira, S., & Faria, R. (2006). Numerical simulation of collapse scenarios in reduced scale tests of arch dams. *Engineering Structures*, *28*(10), 1430-1439. https://doi.org/10.1016/j.engstruct.2006.01.012

Owen, A. B. (2014). Sobol' Indices and Shapley Value. *SIAM/ASA Journal on Uncertainty Quantification*, *2*(1), 245-251. https://doi.org/10.1137/130936233

Papaioannou, I., & Straub, D. (2021). Variance-based reliability sensitivity analysis and the FORM α-factors. *Reliability Engineering & System Safety*, *210*, 107496. https://doi.org/10.1016/j.ress.2021.107496

Parisi, P., Moustapha, M., Marelli, S., & Sudret, B. (2022). *Active learning for system reliability analysis using PC-Kriging, subset simulation and sensitivity analysis*. https://doi.org/10.3850/978-981-18-5184-1_MS-16-193-cd

Patil, S. R., & Frey, C. H. (2004). Comparison of Sensitivity Analysis Methods Based on Applications to a Food Safety Risk Assessment Model. *Risk Analysis*, *24*(3), 573-585. https://doi.org/10.1111/j.0272-4332.2004.00460.x

Pereira, R., Batista, A. L., Neves, L. C., & Lemos, J. V. (2022). Deduction of ultimate equilibrium limit states for concrete gravity dams keyed into rock mass foundations based on large displacement analysis. *Structures*, *38*, 1180-1190. https://doi.org/10.1016/j.istruc.2022.02.049

Periçaro, G. A., Santos, S. R., Ribeiro, A. A., & Matioli, L. C. (2015). HLRF–BFGS optimization algorithm for structural reliability. *Applied Mathematical Modelling*, *39*(7), 2025-2035. https://doi.org/10.1016/j.apm.2014.10.024

Plizzari, G., Waggoner, F., & Saouma, V. E. (1995). Centrifuge Modeling and Analysis of Concrete Gravity Dams. *Journal of Structural Engineering*, *121*(10), 1471-1479. https://doi.org/10.1061/(ASCE)0733-9445(1995)121:10(1471)

Przemyslaw, Z. (2021, Feb 24-27). *Risk analysis in dam safety: The past, the present and the future* 92nd ICOLD Annual Meeting & International Symposium on "Dams for People, Water, Environment and Development", New Delhi, India.

Rackwitz, R., & Fiessler, B. (1978). Structural reliability under combined random load sequences. *Computers & Structures*, *9*(5), 489-494. https://doi.org/10.1016/0045-7949(78)90046-9

Regina, S., Matioli, L., & Beck, A. (2012). New optimization algorithms for structural reliability. *Comput Model Eng Sci*, *83*, 23-55.

Reinius, E. (1962). *Vattenbyggnad del 3 – Dammbyggnader.*

RIDAS. (2025). *RIDAS - Energiföretagens riktlinjer för dammsäkerhet.*

Rosenblatt, M. (1952). Remarks on a Multivariate Transformation. *The Annals of Mathematical Statistics*, *23*(3), 470 - 472. https://doi.org/10.1214/aoms/1177729394

Roudak, M. A., Shayanfar, M. A., Barkhordari, M. A., & Karamloo, M. (2017). A robust approximation method for nonlinear cases of structural reliability analysis. *International Journal of Mechanical Sciences*, *133*, 11-20. https://doi.org/10.1016/j.ijmecsci.2017.08.038

Roussouly, N., Petitjean, F., & Salaun, M. (2013). A new adaptive response surface method for reliability analysis. *Probabilistic Engineering Mechanics*, *32*, 103-115. https://doi.org/10.1016/j.probengmech.2012.10.001

Roy, A., & Chakraborty, S. (2023). Support vector machine in structural reliability analysis: A review. *Reliability Engineering & System Safety*, *233*, 109126. https://doi.org/10.1016/j.ress.2023.109126

Ruggeri, G., Pellegrini, R., Rubin de Celix, M., Berntsen, M., Royet, P., Bettzieche, V., Amberg, W., Gustaffsson, A., Morison, T., & Zenz, G. (2004). *Sliding Safety of Existing Gravity Dams, Final Report.*

Saichi, T., & Bouaanani, N. (2024). Contribution of 3D Roughness Along Concrete-Rock Interface to the Sliding Stability of Concrete Gravity Dams. *Geotechnical and Geological Engineering*, *42*(5), 3805-3827. https://doi.org/10.1007/s10706-024-02758-9

Saichi, T., Renaud, S., Bouaanani, N., & Miquel, B. (2019). Effects of Rock Foundation Roughness on the Sliding Stability of Concrete Gravity Dams Based on Topographic Surveys. *Journal of Engineering Mechanics*, *145*(7), 04019043. https://doi.org/10.1061/(ASCE)EM.1943-7889.0001604

Saltelli, A. (2004). Global sensitivity analysis: an introduction. Proc. 4th international conference on sensitivity analysis of model output (SAMO'04),

Saltelli, A., & Annoni, P. (2010). How to avoid a perfunctory sensitivity analysis. *Environmental Modelling & Software*, *25*(12), 1508-1517. https://doi.org/10.1016/j.envsoft.2010.04.012

Saltelli, A., Bammer, G., Bruno, I., Charters, E., Fiore, M., Didier, E., Espeland, W., Kay, J., Lo Piano, S., Mayo, D., Jr, R., Portaluri, T., Porter, T., Puy, A., Rafols, I., Ravetz, J., Reinert, E., Sarewitz, D., Stark, P., & Vineis, P. (2020). Five ways to ensure that models serve society: a manifesto. *Nature*, *582*, 482-484. https://doi.org/10.1038/d41586-020-01812-9

Saltelli, A., Ratto, M., Andres, T., Campolongo, F., Cariboni, J., Gatelli, D., Saisana, M., & Tarantola, S. (2008). *Global Sensitivity Analysis. The Primer* (Vol. 304). https://doi.org/10.1002/9780470725184.ch6

Saltelli, A., Tarantola, S., & Campolongo, F. (2000). Sensitivity Analysis as an Ingredient of Modeling. *Statistical Science*, *15*(4), 377-395. http://www.jstor.org/stable/2676831

Samarakoon, S. M. K., & Ratnayake, R. M. C. (2015). Strengthening, modification and repair techniques' prioritization for structural integrity control of ageing offshore structures. *Reliability Engineering & System Safety*, *135*, 15-26. https://doi.org/10.1016/j.ress.2014.10.023

Saraygord Afshari, S., Enayatollahi, F., Xu, X., & Liang, X. (2022). Machine learning-based methods in structural reliability analysis: A review. *Reliability Engineering & System Safety*, *219*, 108223. https://doi.org/10.1016/j.ress.2021.108223

Sarmiento, S. J., O'Connor, A., González-Libreros, J., & Sas, G. (2025). An Improved Metamodel-Based Algorithm Using Copula Theory for Assessing Reliability Analysis of Structures using FEM. *Structural Engineering International*, 1-14. https://doi.org/10.1080/10168664.2025.2517059

Sas, G., Popescu, C., Bista, D., Seger, A., Arntsen, B., Johansson, F., & Lia, L. (2021). Influence of large-scale asperities on the shear strength of concrete-rock interface of small buttress dams. *Engineering Structures*, *245*, 112952. https://doi.org/10.1016/j.engstruct.2021.112952

Schöbi, R. (2017). *Surrogate models for uncertainty quantification in the context of imprecise probability modelling* [Doctoral Thesis, ETH Zürich]. Zurich, Switzerland.

Schöbi, R., & Sudret, B. (2014). *PC-Kriging: A new metamodelling method combining Polynomial Chaos Expansions and Kriging* Proceedings of the 2nd International Symposium on Uncertainty Quantification and Stochastic Modeling, Rouen, France.

Schöbi, R., Sudret, B., & Marelli, S. (2017). Rare Event Estimation Using Polynomial-Chaos Kriging. *ASCE-ASME Journal of Risk and Uncertainty in Engineering Systems, Part A: Civil Engineering*, *3*(2), D4016002. https://doi.org/10.1061/AJRUA6.0000870

Schöbi, R., Sudret, B., & Wiart, J. (2015). Polynomial-Chaos-Based Kriging. *International Journal of Uncertainty Quantification*, *5*. https://doi.org/10.1615/Int.J.UncertaintyQuantification.2015012467

Schuëller, G. I., Bucher, C. G., Bourgund, U., & Ouypornprasert, W. (1989). On efficient computational schemes to calculate structural failure probabilities. *Probabilistic Engineering Mechanics*, *4*(1), 10-18. https://doi.org/10.1016/0266-8920(89)90003-9

Segura, R., Padgett, J. E., & Paultre, P. (2020). Metamodel-Based Seismic Fragility Analysis of Concrete Gravity Dams. *Journal of Structural Engineering*, *146*(7), 04020121. https://doi.org/10.1061/(ASCE)ST.1943-541X.0002629

Soares do Amaral, J. V., Montevechi, J. A. B., Miranda, R. d. C., & Junior, W. T. d. S. (2022). Metamodel-based simulation optimization: A systematic literature review. *Simulation Modelling Practice and Theory*, *114*, 102403. https://doi.org/10.1016/j.simpat.2021.102403

Sobol', I. M. (1967). On the distribution of points in a cube and the approximate evaluation of integrals. *USSR Computational Mathematics and Mathematical Physics*, 7(4), 86-112. https://doi.org/10.1016/0041-5553(67)90144-9

Sobol', I. M. (1993). Sensitivity analysis for non-linear mathematical models. *Mathematical Modelling and Computational Experiment*, *1*, 407–414.

Soltani, N., Escuder-Bueno, I., & Klun, M. (2024). System Reliability Analysis of Concrete Arch Dams Considering Foundation Rock Wedges Movement: A Discussion on the Limit Equilibrium Method. *Infrastructures*, *9*(10), 176. https://www.mdpi.com/2412-3811/9/10/176

Song, C., & Kawai, R. (2023). Monte Carlo and variance reduction methods for structural reliability analysis: A comprehensive review. *Probabilistic Engineering Mechanics*, *73*, 103479. https://doi.org/10.1016/j.probengmech.2023.103479

Sonin, A. (2001). *The Physical Basis of Dimensional analysis* (2nd ed.). Department of Mechanical Engineering, MIT, Cambridge.

Stimpson, B. (1970). Modelling materials for engineering rock mechanics. *International Journal of Rock Mechanics and Mining Sciences & Geomechanics Abstracts*, 7(1), 77-121. https://doi.org/10.1016/0148-9062(70)90029-X

Stone, M. (1974). Cross-Validatory Choice and Assessment of Statistical Predictions. *Journal of the Royal Statistical Society. Series B (Methodological)*, *36*(2), 111-147. http://www.jstor.org/stable/2984809

Su, H., Wen, Z., Zhang, S., & Tian, S. (2016). Method for Choosing the Optimal Resource in Back-Analysis for Multiple Material Parameters of a Dam and Its Foundation. *Journal of Computing in Civil Engineering*, *30*(4), 04015060. https://doi.org/10.1061/(ASCE)CP.1943-5487.0000537

Sudret, B. (2012). *Meta-models for structural reliability and uncertainty quantification* Asian-Pacific Symposium on Structural Reliability and its Applications, Singapore, Singapore.

Sudret, B. (2014). Polynomial chaos expansions and stochastic finite element methods. In K.-K. Phoon & J. Ching (Eds.), *Risk and Reliability in Geotechnical Engineering* (pp. 265-300). CRC Press.

Sudret, B. (2015). Polynomial chaos expansions and stochastic finite element methods. In J. C. Kok-Kwang Phoon (Ed.), *Risk and Reliability in Geotechnical Engineering* (pp. 265-300). CRC Press. https://hal.science/hal-01449883

Sudret, B., & Der Kiureghian, A. (2000). *Stochastic Finite Element Methods and Reliability A State-of-the-Art Report*.

Sudret, B., & Mai, C. V. (2015). Computing derivative-based global sensitivity measures using polynomial chaos expansions. *Reliability Engineering & System Safety*, *134*, 241-250. https://doi.org/10.1016/j.ress.2014.07.009

Teixeira, R., Nogal, M., & O'Connor, A. (2021). Adaptive approaches in metamodel-based reliability analysis: A review. *Structural Safety*, *89*, 102019. https://doi.org/10.1016/j.strusafe.2020.102019

Tvedt, L. (1990). Distribution of Quadratic Forms in Normal Space - Application to Structural Reliability. *Journal of Engineering Mechanics*, *116*(6), 1183-1197. https://doi.org/10.1061/(ASCE)0733-9399(1990)116:6(1183)

Ulfberg, A., González-Libreros, J., Das, O., Malm, R., Johansson, F., Westberg Wilde, M., & Sas, G. (2023). *On the applicability of scale model tests for concrete dams: A review* 91st Annual ICOLD Meeting, Gothenburg.

Ulfberg, A., González-Libreros, J., Das, O., Sas, G., Andersson, E., Bista, D., Arntsen, B., & Seger, A. (2022). *Influence of large-scale asperities on the stability of concrete dams* IABSE Symposium: Challenges for Existing and Oncoming Structures, Prague.

USACE. (1995). *Gravity dam design.*

USACE. (2005). *Stability analysis of concrete structures.*

Vrouwenvelder, T., Baker, M., & Faber, M. H. (2025). The JCSS – A major contributor to structural safety through half a century. *Structural Safety*, *113*, 102468. https://doi.org/10.1016/j.strusafe.2024.102468

Wang, Z., & Wang, P. (2013). A Maximum Confidence Enhancement Based Sequential Sampling Scheme for Simulation-Based Design. *Journal of Mechanical Design*, *136*(2). https://doi.org/10.1115/1.4026033

Wei, P., Lu, Z., & Yuan, X. (2013). Monte Carlo simulation for moment-independent sensitivity analysis. *Reliability Engineering & System Safety*, *110*, 60-67. https://doi.org/10.1016/j.ress.2012.09.005

Westberg Wilde, M., & Johansson, F. (2016a). *Probabilistic Model Code for Concrete Dams - Part I, Part II, Part III and example.*

Westberg Wilde, M., & Johansson, F. (2016b). *Sannolikhetsbaserad bedömning av betongdammars stabilitet.*

Wieland, M., & Mueller, R. (2009). Dam safety, emergency action plans and water alarm systems. *61*, 34-38.

Wu, H., Chen, Z. Q., & Cheng, Y. H. (2025). Influence of explosion position on blast resistance of concrete gravity dam against underwater explosion blast wave and bubble pulsation. *Engineering Failure Analysis*, *169*, 109188. https://doi.org/10.1016/j.engfailanal.2024.109188

Xiong, J., Lu, W., Wang, G., Chen, M., Wang, Y., & Liu, J. (2024). Vertical crack identification of arch dam under underwater explosion based on mode transition. *Structures*, *59*, 105671. https://doi.org/10.1016/j.istruc.2023.105671

Xu, B., & Wang, S.-d. (2023). Sensitivity analysis of factors affecting gravity dam anti-sliding stability along a foundation surface using Sobol method. *Water Science and Engineering*, *16*(4), 399-407. https://doi.org/10.1016/j.wse.2023.10.001

Xu, Z., & Saleh, J. H. (2021). Machine learning for reliability engineering and safety applications: Review of current status and future opportunities. *Reliability*

Engineering & System Safety, *211*, 107530. https://doi.org/10.1016/j.ress.2021.107530

Yang, B., Zhang, L., Liu, E., Dong, J., Zhu, H., & Chen, Y. (2015). Deformation Monitoring of Geomechanical Model Test and Its Application in Overall Stability Analysis of a High Arch Dam. *Journal of Sensors*, *2015*, 470905. https://doi.org/10.1155/2015/470905

Yang, D. (2010). Chaos control for numerical instability of first order reliability method. *Communications in Nonlinear Science and Numerical Simulation*, *15*(10), 3131-3141. https://doi.org/10.1016/j.cnsns.2009.10.018

Yun, W., Lu, Z., Feng, K., & Li, L. (2019). An elaborate algorithm for analyzing the Borgonovo moment-independent sensitivity by replacing the probability density function estimation with the probability estimation. *Reliability Engineering & System Safety*, *189*, 99-108. https://doi.org/10.1016/j.ress.2019.04.015

Yun, W., Lu, Z., Jiang, X., & Zhang, L. (2018). Borgonovo moment independent global sensitivity analysis by Gaussian radial basis function meta-model. *Applied Mathematical Modelling*, *54*, 378-392. https://doi.org/10.1016/j.apm.2017.09.048

Yun, W., Lu, Z., Jiang, X., Zhang, L., & He, P. (2020). AK-ARBIS: An improved AK-MCS based on the adaptive radial-based importance sampling for small failure probability. *Structural Safety*, *82*, 101891. https://doi.org/10.1016/j.strusafe.2019.101891

Zhang, L., Liu, X., Chen, J., & Hu, C. (2004). The Geomechanical Model Test on Stability of Arch Dam Abutment under Complex Geological Conditions. *Journal of Sichuan university*, *36*(6).

Zhang, W., Guan, Y., Wang, Z., & Xu, H. (2025). A novel active learning Kriging based on improved Metropolis-Hastings and importance sampling for small failure probabilities. *Computer Methods in Applied Mechanics and Engineering*, *435*, 117658. https://doi.org/10.1016/j.cma.2024.117658

Zhang, Y., & Der Kiureghian, A. (1994). Two lmproved Algorithms for Reliability Analysis.*IFIP Advances in Information and Communication Technology* Reliability and Optimization of Structural Systems, Assisi, Italy.

Zhang, Y., Huang, H., Xiong, M., & Yao, Z. (2023). A PC-kriging-HDMR Integrated with an Adaptive Sequential Sampling Strategy for High-Dimensional Approximate Modeling. *International Journal of Computer Science and Information Technology*, *15*, 63-79. https://doi.org/10.5121/ijcsit.2023.15305

Zhang, Y., Liu, Y., Tao, Z., Zhou, H., & Yang, Q. (2019). Fractal Characteristics and Failure Analysis of Geomechanical Model for Arch Dam Based on Acoustic Emission Technique. *International Journal of Geomechanics*, *19*(11), 04019119. https://doi.org/10.1061/(ASCE)GM.1943-5622.0001502

Zhou, T., & Peng, Y. (2022). Reliability analysis using adaptive Polynomial-Chaos Kriging and probability density evolution method. *Reliability Engineering & System Safety*, *220*, 108283. https://doi.org/10.1016/j.ress.2021.108283

Zhu, S.-P., Keshtegar, B., Ben Seghier, M. E. A., Zio, E., & Taylan, O. (2022). Hybrid and enhanced PSO: Novel first order reliability method-based hybrid intelligent approaches. *Computer Methods in Applied Mechanics and Engineering*, *393*, 114730. https://doi.org/10.1016/j.cma.2022.114730

Department of Civil, Environmental and Natural Resources Engineering
Division of Structural and Fire Engineering

ISSN 1402-1544
ISBN 978-91-8048-953-9 (print)
ISBN 978-91-8048-954-6 (pdf)

Luleå University of Technology 2026